Recent changes in the Southern Annular Mode are associated with warmer, drier conditions in the Southern Hemisphere. An analysis of tree-ring records there suggests that these changes have significantly altered tree growth. The image shows a millennial-aged cypress tree of the species *Austrocedrus chilensis* in the northern Patagonian Andes

Cover image: Duncan Christie
Cover Design: Karen Moore

nature geoscience

LETTERS

PUBLISHED ONLINE: 28 OCTOBER 2012 | DOI: 10.1038/NGEO1613

Unusual Southern Hemisphere tree growth patterns induced by changes in the Southern Annular Mode

Ricardo Villalba[1]*, Antonio Lara[2], Mariano H. Masiokas[1], Rocío Urrutia[2], Brian H. Luckman[3], Gareth J. Marshall[4], Ignacio A. Mundo[1], Duncan A. Christie[2], Edward R. Cook[5], Raphael Neukom[6,7], Kathryn Allen[8], Pavla Fenwick[9], José A. Boninsegna[1], Ana M. Srur[1], Mariano S. Morales[1], Diego Araneo[1], Jonathan G. Palmer[9], Emilio Cuq[2], Juan C. Aravena[10], Andrés Holz[11] and Carlos LeQuesne[2]

Recent changes in the summer climate of the Southern Hemisphere extra-tropics are primarily related to the dominance of the positive phase of the Southern Annular Mode[1,2]. This shift in the behaviour of the Southern Annular Mode—essentially a measure of the pressure gradient between Southern Hemisphere mid and high latitudes—has been predominantly induced by polar stratospheric ozone depletion[2–4]. The concomitant southward expansion of the dry subtropical belts[5,6] could have consequences for forest growth. Here, we use tree-ring records from over 3,000 trees in South America, Tasmania and New Zealand to identify dominant patterns of tree growth in recent centuries. We show that the foremost patterns of growth between 1950 and 2000 differed significantly from those in the previous 250 years. Specifically, growth was higher than the long-term average in the subalpine forests of Tasmania and New Zealand, but lower in the dry-mesic forests of Patagonia. We further demonstrate that variations in the Southern Annular Mode can explain 12–48% of the tree growth anomalies in the latter half of the twentieth century. Tree-ring-based reconstructions of summer Southern Annular Mode indices suggest that the high frequency of the positive phase since the 1950s is unprecedented in the past 600 years. We propose that changes in the Southern Annular Mode have significantly altered tree growth patterns in the Southern Hemisphere.

The most robust and significant change in the Southern Hemisphere atmospheric circulation over recent decades has been the increase in the difference in the mean zonal pressure at sea level between mid and high latitudes[1,2]. These changes in the pressure fields are well reflected in the increase of the positive phase of the Southern Annular Mode (SAM), also called the Antarctic Oscillation[1,7]. The persistent positive trend of the SAM in recent decades has been related to a shift to higher latitudes of the Westerlies and associated storm tracks, the poleward migration of the descending branch of the Hadley cell, and the consequent southern expansion of the dry subtropical belts[2,5,6]. Several studies have reported significant anomalies in regional temperature and precipitation changes in most Southern Hemisphere continents that are related to changes in the SAM (refs 2,8–11). Tree growth patterns in some specific regions have also been related to inter-annual changes in the SAM (ref. 12). However, no detailed assessment has been carried out of the large-scale impacts of these recent changes in the SAM on the Southern Hemisphere forests or the relative magnitude of these changes in a long-term, multi-century context.

At regional and continental scales, climate is the main driver of forest growth[13,14]. Tree-ring chronologies provide valuable records of tree growth owing to their annual resolution, wide geographic distribution and temporal coverage over century to millennial timescales[15]. The pace of development of tree-ring chronologies has been exponential in the Southern Hemisphere, especially during the past two decades, providing new and updated tree-ring records across South America, Tasmania and New Zealand[16–18]. Using the largest and most updated network of chronologies available at present for the Southern Hemisphere, we identified regional tree growth patterns for the temperate forests in these three regions during the past 4–600 years (see Supplementary Table S1). The initial analyses of the raw tree-ring width data reveal that the dominant patterns of regional growth observed since the 1950s are significantly different from those recorded in the previous 250 years. Temperate, dry–mesic forests in southern South America show a marked decreasing growth trend over the past five decades that contrasts with the increasing trend recorded in the subalpine trees from Tasmania and New Zealand (Fig. 1).

Regional growth records for each species were developed by merging those individual site chronologies that share a large percentage of common variance. Standardized regional chronologies show that the anomalous tree ring patterns observed

[1]Instituto Argentino de Nivología, Glaciología y Ciencias Ambientales, CONICET, CCT-Mendoza, Casilla de Correo 330, 5500 Mendoza, Argentina, [2]Laboratorio de Dendrocronología y Cambio Global, Facultad de Ciencias Forestales y Recursos Naturales, Universidad Austral de Chile, Casilla 567, Valdivia, Chile, [3]Department of Geography, University of Western Ontario, London, Ontario N6A 3K1, Canada, [4]British Antarctic Survey, Cambridge, CB3 0ET, UK, [5]Lamont-Doherty Earth Observatory of Columbia University, Palisades, New York 10964, USA, [6]Oeschger Centre for Climate Change Research, University of Bern, 3012 Bern, Switzerland, [7]Swiss Federal Research Institute WSL, 8903 Birmensdorf, Switzerland, [8]Biological Sciences, Monash University, 310 Blackburn Road, Clayton, Victoria 3800, Australia, [9]Gondwana Tree-ring Laboratory, PO Box 14, Little River, Canterbury 7546, New Zealand, [10]Centro de Estudios del Cuaternario, 21 de Mayo 1690, Casilla 737, Punta Arenas, Chile, [11]School of Plant Science, University of Tasmania, Hobart 7001, Tasmania, Australia. *e-mail: ricardo@mendoza-conicet.gob.ar.

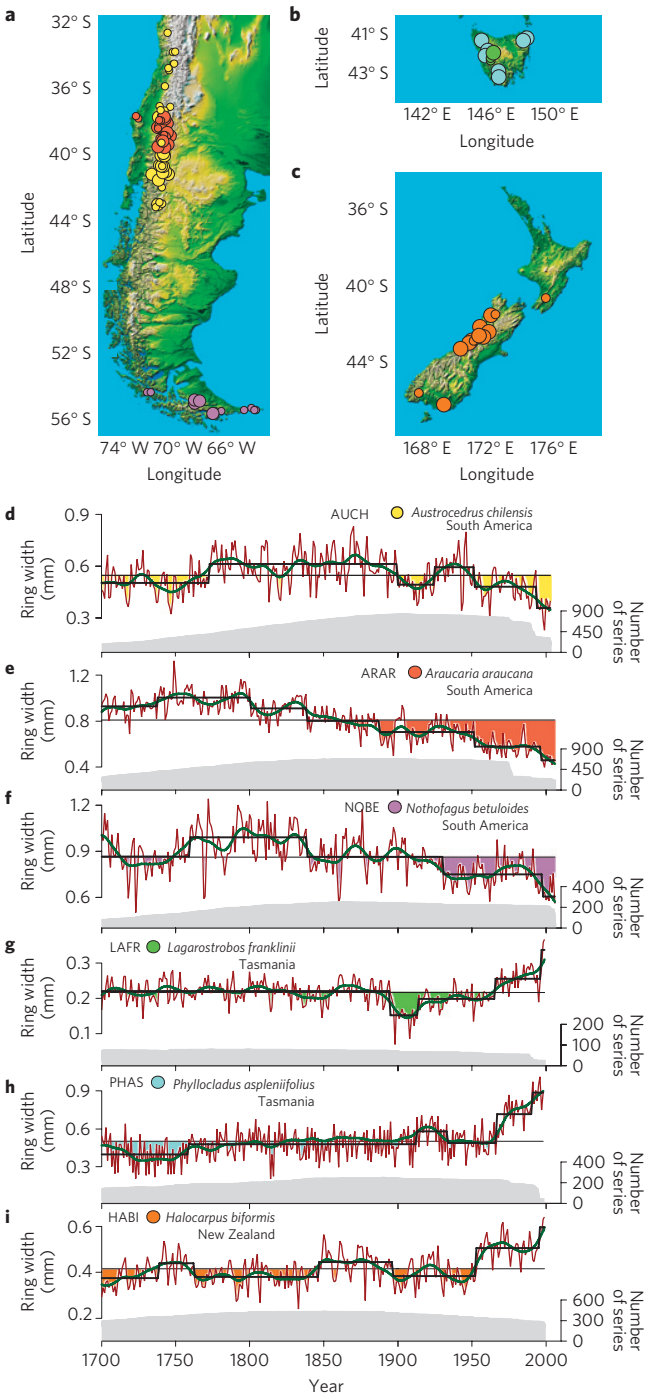

Figure 1 | Long-term variations in tree growth at mid latitudes in the Southern Hemisphere. a–c, Location of tree-ring chronologies. Chronologies strongly contributing to dominant patterns of tree growth at subcontinental scales are shown with larger circles. **d–i**, Variations in non-standardized regional chronologies since AD 1700. The thick green line emphasizes long-term variations in the raw ring widths. Mean regime levels in tree growth (black lines) were determined using a robust shift detection technique[30]. The number of tree-ring series in the regional annual means is also shown. Note the recent extreme negative (positive) growth anomalies in Patagonia (Tasmania–New Zealand).

over recent decades were strongly related to regional hydroclimatic records and to the large-scale climatic indices traditionally used to account for variations in the extra-tropical atmospheric circulation in the Southern Hemisphere. Remarkable similarities are observed between long-term tree growth, climate and the summer SAM index trends during the past 50 years (Fig. 2 and Supplementary Table S3). Recent changes in the radial growth of *Austrocedrus chilensis* and *Araucaria araucana* trees in northwestern Patagonia reflect the gradual decrease in water available at the sampling sites as revealed by significant relationships between tree growth and summer runoff, an integrative estimate of moisture at regional scales (Fig. 2g,h). In southernmost South America, the radial growth of *Nothofagus betuloides* trees has a significant and negative relationship with regional temperatures (that is, suppressed growth during warm years and vice versa), also suggesting that water supply plays a dominant role modulating tree growth at these southern locations (Fig. 2i). The negative correlations of *Austrocedrus*, *Araucaria* and *Nothofagus* tree growth in South America with the SAM index (Fig. 2m–o) are consistent with the decrease in precipitation induced by the SAM in the Patagonian Andes[9–11]. Growth variations of *Lagarostrobos franklinii* and *Phyllocladus aspleniifolius* trees in Tasmania and *Halocarpus biformis* trees in New Zealand are statistically significantly correlated with temperature changes during the twentieth century in both regions[16,18] (Fig. 2j–l), which may be in turn partially due to persistent, positive SAM anomalies over the past decades[11,19] (Fig. 2d–f). In addition, significant relationships have also been recorded between the regional chronologies and the SAM indices reconstructed from the few series of atmospheric pressure available for the mid latitudes in the Southern Hemisphere since the late 1800s (refs 20,21; Fig. 3 and Supplementary Table S3). As shown in Fig. 3a,b,d, trends in tree growth and climate in the Southern Hemisphere mid latitudes are consistent with the climatic anomalies produced by the persistently positive phase of the SAM since the mid 1950s. The significant increase in the atmospheric pressure at mid latitudes of the Southern Hemisphere has been associated with a weakening of the westerly winds, a lower frequency of moisture-laden masses of Pacific origin in South America and a greater number of warm subtropical air masses across New Zealand[2].

Regression techniques indicate that percentages as high (low) as 48 and 33% (20 and 14%) of the total variance in tree growth variations could be explained by the SAM for the South American and New Zealand forests, respectively (Fig. 2m–o,r). The *Lagarostrobos* and *Phyllocladus* regional records from Tasmania show clear increasing trends during the past decades that we initially related to the positive long-term trend observed in the SAM. However, we noted that the influence of SAM on the radial growth of these species substantially decreases after accounting for autocorrelation in the series, suggesting that a large portion of the significant relationships could be due to the persistent positive trends in both the tree-ring and SAM records (Fig. 2p,q). This suggests that other climatic forcings also play a significant role in modulating the growth of the forests in Tasmania. The weaker relationships observed between records in Tasmania and the SAM are consistent with climatic studies indicating that the warming across Australia during the twentieth century is mainly related to anthropogenic greenhouse gases and sulphate aerosols[22]. It has been postulated that SAM could have mitigated summer warming in Tasmania[2,19]. Interestingly, no patterns of significant correlations were recorded between tree growth in the temperate Southern Hemisphere and tropical climatic drivers measured through the Southern Oscillation Index (Supplementary Table S3), suggesting that tree growth in many areas at mid latitudes is largely influenced by extra-tropical circulation.

The tree-ring records discussed in this paper provide a long-term perspective of the common variation in forest growth at mid latitudes in the Southern Hemisphere. The strong relationships observed between these regionally representative records and the SAM series offer the unique opportunity of using the tree-ring

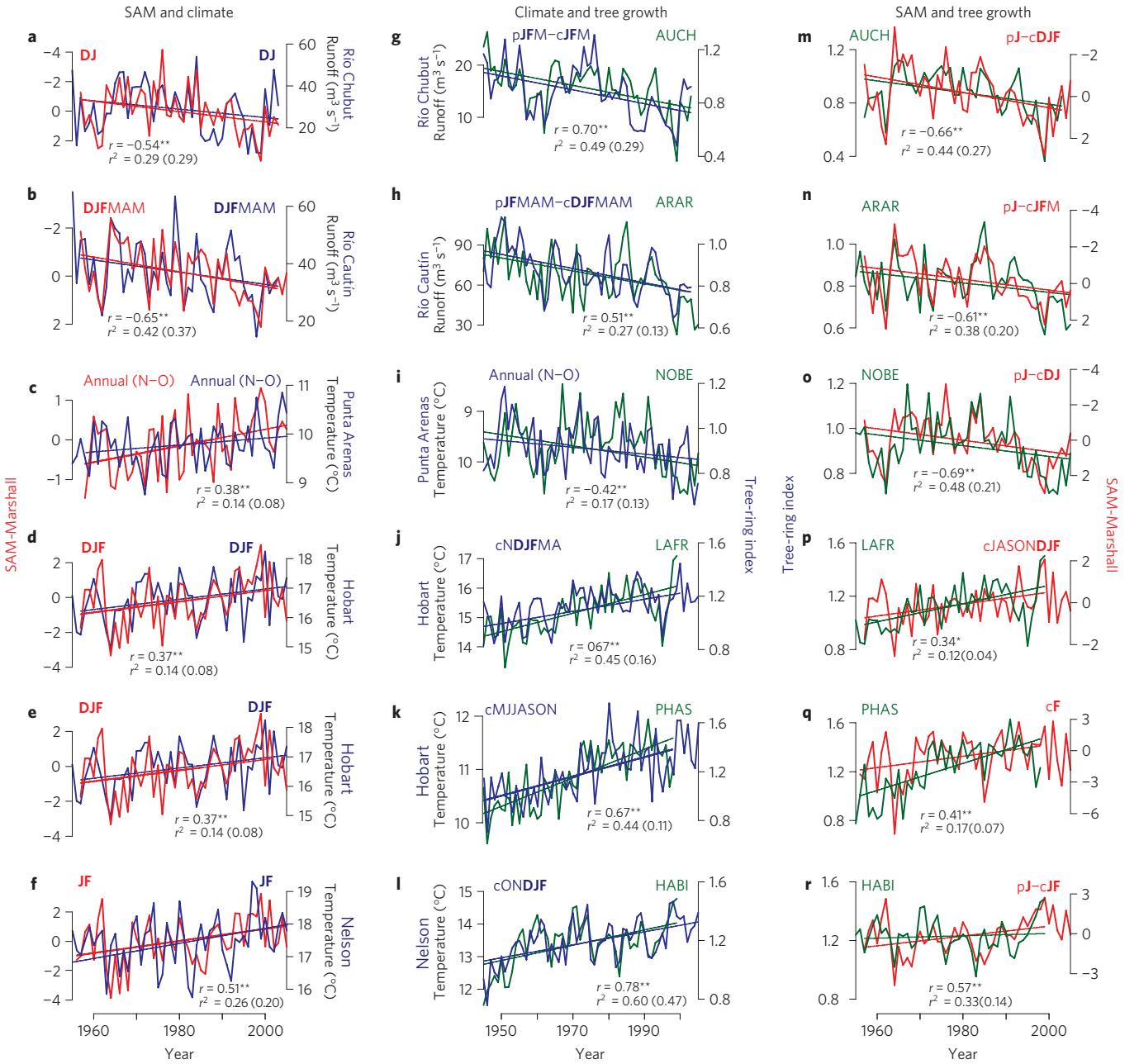

Figure 2 | Influences of the SAM on regional climate and forest growth. a–r, Variables shown include the SAM indices (**a–f**, **m–r**; red lines), hydro-climatic variables (**a–l**; blue lines) and tree-ring indices (**g–r**; green lines). The left and right columns show correlation coefficients and the percentage of total variance in regional climate and forest growth explained by the SAM. The central column shows similar results for radial growth and regional hydro-meteorological variables. Maximum and minimum (in parentheses) percentages of total variance estimated using the original and the linear-trend-removed series are indicated. Owing to preconditioning of tree growth[15], tree-ring series were compared with climate and the SAM during current (c) and previous (p) growing seasons. SAM indices are plotted inversely in **a**, **b** and **m–o**. Significance at 99% (**) and 95% (*) confidence levels is indicated. Austral summer months (DJF) are highlighted in each seasonal composite.

records as proxy indicators of changes in the SAM during the past centuries. Using time-varying subsets of regional chronologies as predictors, we develop two reconstructions of mean summer (December–February) SAM variations for the period 1409–2006. Two instrumental target series were selected for analysis: the SAM-Marshall[7] (based on selected station pressure records) and the SAM-NCEP (ref. 1; based on mean sea-level pressure south of 20°S; Fig. 4). The first principal component (PC1) of the three regional chronologies best correlated with the predictands (Fig. 3 and Supplementary Table S3) explains 44 and 47% of the total variance of the SAM-Marshall and SAM-NCEP instrumental records, respectively (Fig. 4 and Supplementary Table S4). The *Araucaria* regional chronology is the longest record available and alone accounts for 24 and 29% of the total variations in the SAM-Marshall and SAM-NCEP indices, respectively. This regional chronology is used to estimate the SAM variations during the earliest period 1409–1485. For the common period of the three regional chronologies (1559–1999), the mean correlation between the *Araucaria* series and the PC1 based on the *Austrocedrus* and *Halocarpus* chronologies is $r = 0.54$ ($n = 441$, $p < 0.001$), an indication of the high temporal stability between the different predictors used for the reconstruction of the SAM. The temporal

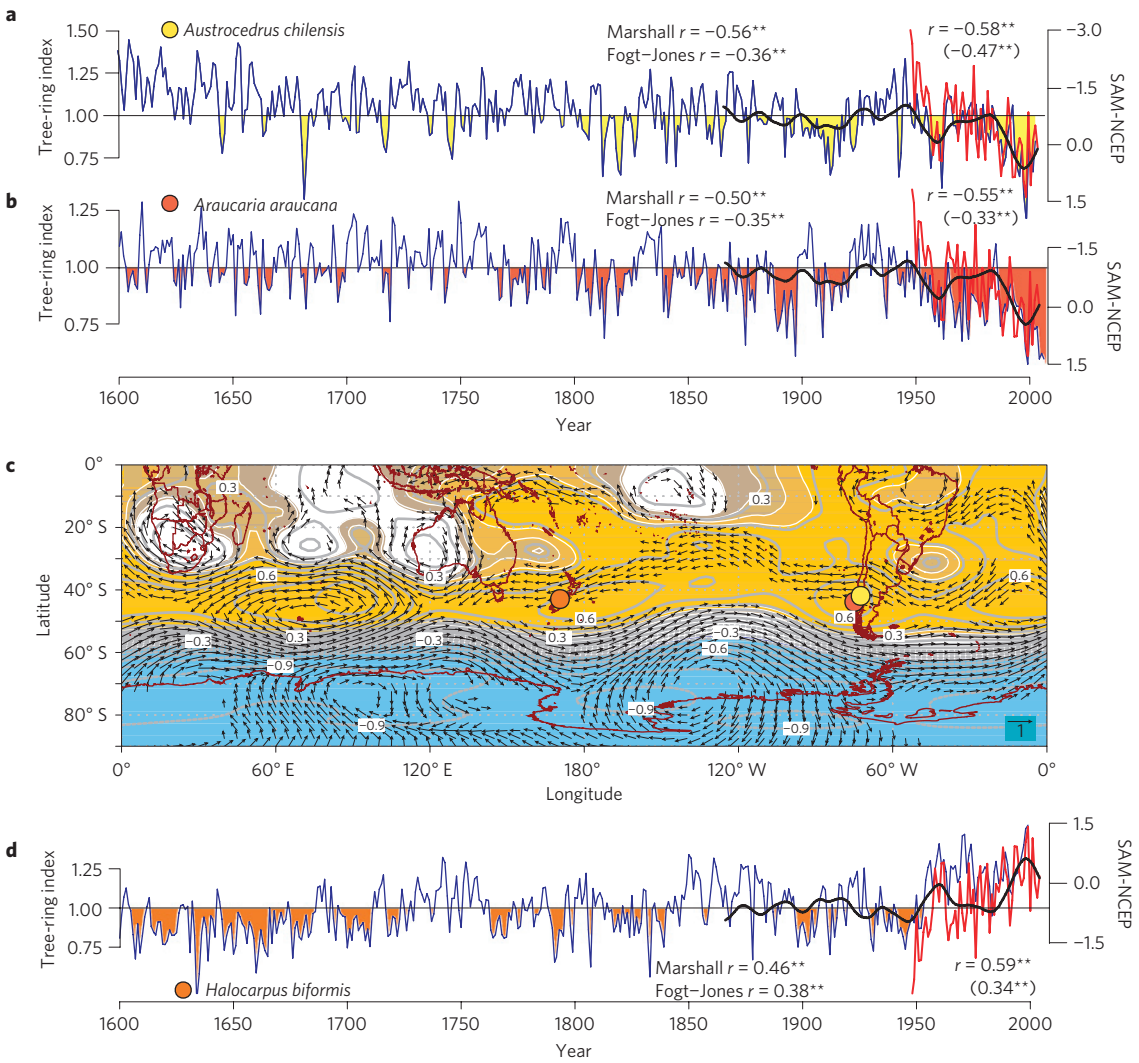

Figure 3 | Variations in regional tree-ring chronologies and the summer SAM. a,**b**,**d**, Tree-ring variations since AD 1600 for the three regional chronologies most closely associated with the summer SAM-NCEP (ref. 1; red) and the smoothed mean of the instrumental-based SAM-Fogt[21]/SAM-Jones[20] index reconstructions (black). SAM indices are plotted inversely in **a** and **b**. Correlation coefficients over the common period are shown for actual and (trend-removed) series. Coefficients are significant at the 99% confidence level. **c**, Summer correlation fields (1948–2004) between the SAM-NCEP index and mean geopotential heights and wind vectors at 500 hPa. Coloured areas correspond to significant geopotential values at 90 (grey-brown), 95 (brown), 97.5 (brown-orange) and 99% (orange or light blue) confidence levels. Only wind correlation vectors with at least one significant component—**u** (zonal) or **v** (meridional)—at the 95% level are shown. For scale, wind vector (arrow) is at the bottom right. Locations of forests are indicated by circles.

stability and robustness of the SAM reconstructions are also reflected in the high reduction of error (RE) statistics obtained in the regression trials (Fig. 4 and Supplementary Table S4).

The SAM index reconstructions show that after a period of relatively high values during the first half of the fifteenth century, the most extreme negative values of the past 600 years occurred around AD 1470. The SAM indices gradually increased until AD 1500 but recorded negative values until AD 1630–1650. This long period of relatively strong negative values of the SAM index coincides with the most severe phase of the Little Ice Age in southern South America[23]. Subsequently, the SAM index values gradually increase and remain relatively stable over the eighteenth century. With the exception of three periods of relatively low index values centred on the decades of AD 1800, 1840 and 1900, the nineteenth and early twentieth centuries show the highest SAM indices for the pre-instrumental period. Relatively low indices of the SAM are recorded from the 1930s to mid 1950s, a period characterized by abundant precipitation in northern Patagonia and lower temperatures in New Zealand[18,24]. A finer-scale analysis of the most recent decades indicates that, consistent with the SAM instrumental records, the reconstructions have an initial increase peaking in 1962 with a short decrease centred in 1964–1965. Since this period, both the instrumental and the reconstructed records show a steady increase in trend culminating in 1999–2000 (Fig. 4). Conservative uncertainty boundaries based on a combination of chronology and calibration errors indicate that decadal and longer scale periods (about AD 1450–1680, 1695–1715, 1720–1730, 1785–1800, 1830–1835 and 1930–1940 in the SAM-Marshall reconstruction, and about AD 1425–1800, 1825–1840 and 1925–1950 in the SAM-NCEP reconstruction) significantly differ from the instrumental SAM indices recorded during the most recent decades.

Recent studies based on instrumental records and climatic models reveal that the changes observed in the Southern Hemisphere summer climate during the past five decades have been mainly induced by the ozone depletion in the stratosphere at high latitudes[2–4]. The development of the ozone hole has not only affected the tropopause over Antarctica but has also induced a poleward shift of the westerly jet at mid latitudes (Fig. 3c), the

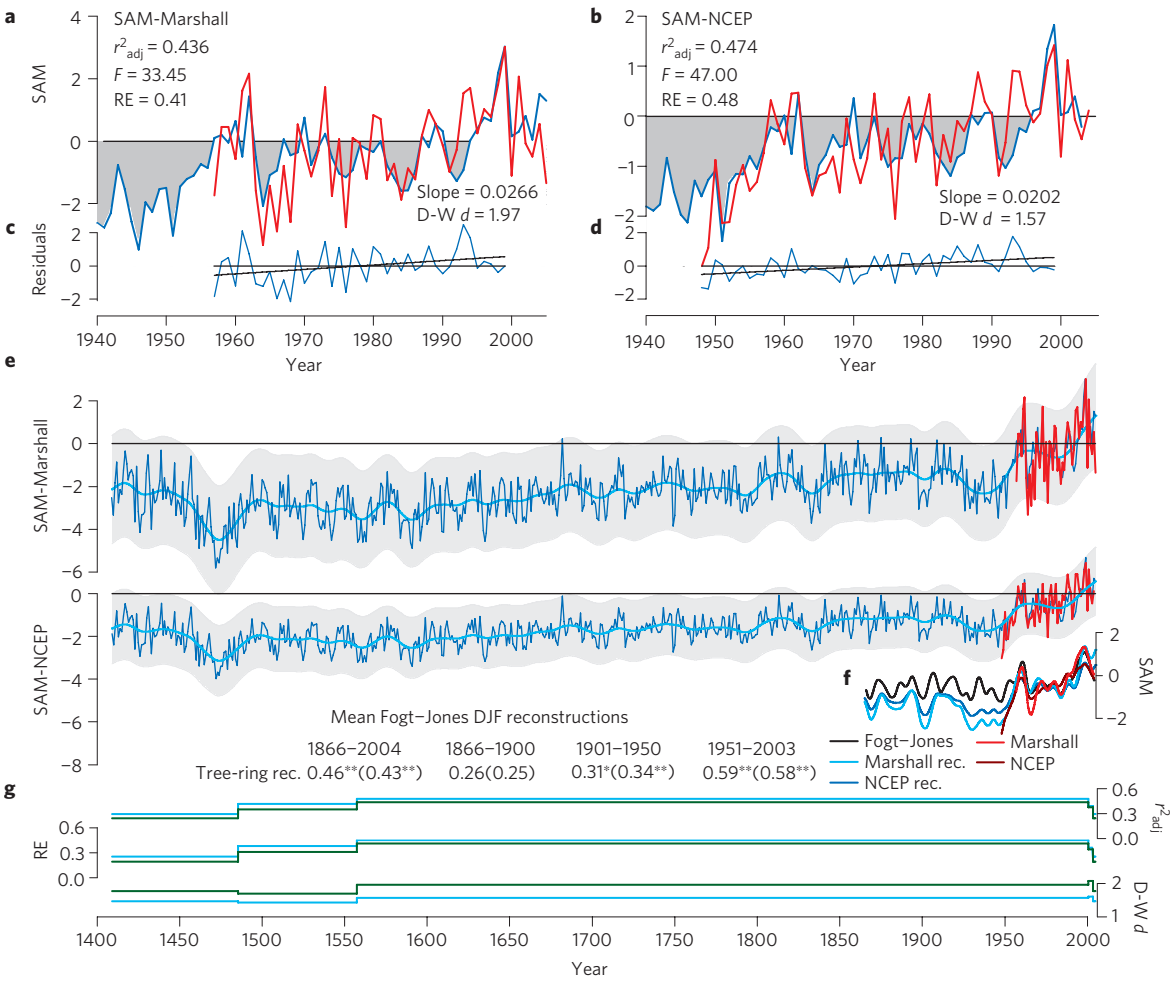

Figure 4 | Summer variations in the SAM for the past 600 years. a–d, Instrumental (red) and tree-ring-based reconstruction (blue) of the summer SAM-Marshall[7] (**a**) and SAM-NCEP (ref. 1; **b**) with regression residuals (**c**,**d**). **e**, Nested reconstructions of the summer SAM-Marshall and summer SAM-NCEP for AD 1409–2006 (thick light blue lines, 30-year spline filter) and associated uncertainty bands (grey areas) integrating chronology and calibration errors. **f**, Comparison between the SAM reconstructions, the mean of the instrumental-based reconstructions of the SAM-Fogt/SAM-Jones and the instrumental records. Correlation coefficients between actual and trend-removed (in parenthesis) series and significance (**99%; *95%) are indicated. **g**, Variations in r^2_{adj}, reduction of error (RE) and the Durbin–Watson (DW) *d* statistic for the SAM-Marshall (green line) and the SAM-NCEP (light blue line) nested models (see Supplementary Table S4 for further information).

displacement of the descending Hadley branch towards higher latitudes, and the poleward migration of the subtropical belts[2,5,6]. The trends in radial growth of temperate forests since the 1950s reflect the drying and warming patterns observed at mid latitudes in the Southern Hemisphere induced by the recent stratospheric ozone depletion and are consistent with the persistently positive increasing trend in the SAM. Our results show that the recent increase in the SAM indices, as well as the changes in tree growth of temperate forests during past 4–5 decades, seem to be unprecedented in the past 600 years. Further research should address the projected influences of the predicted ozone recovery and the increase in greenhouse gases on the atmospheric circulation in the Southern Hemisphere[2,3] to elucidate the future patterns of tree growth in Southern Hemisphere temperate forests, which include some of the longest-lived species in the world that are endangered or threatened at present[16,25].

Methods

Tree-ring records have been used to determine the influences of temperature, precipitation and other climatic factors on forest growth[15]. The database consisted of a recently compiled network of 102 tree-ring sites in the Southern Hemisphere including 39 *Austrocedrus*, 26 *Araucaria*, 13 *Nothofagus*, 14 *Halocarpus*, 7 *Phyllocladus* and 3 *Lagarostrobos* chronologies (Supplementary Table S1). For each species, site chronologies that share a large percentage of common signal in tree-ring variations were merged in regional chronologies. These regional records are well replicated during the 1980s and 1990s allowing identification of tree growth changes over the past 20 years. There is no tree-ring chronology network from southern Africa of comparable quality and length to those of South America, Tasmania and New Zealand, and therefore no records from that region are included in this analysis.

To conserve the low-frequency signal in the tree-ring records, conservative methods of standardization were selected, fitting negative exponential or linear curves with zero or negative slope to each individual series, or by smoothing each series with a robust median filter[26] (for a discussion on the standardization procedures and the different curve fitting see Supplementary Full Methods section and Figs S1–S6).

The SAM-Marshall[7] (based on a selection of pressure station records from mid and high latitudes of the Southern Hemisphere) and the SAM-NCEP (ref. 1; calculated from sea-level pressure anomalies south of 20° S) index reconstructions were developed following a nested linear regression approach intended to maximize the reconstruction length[27,28]. The regression statistics of both reconstructions are included in Fig. 4a,b, and in Supplementary Table S4. With the exception of the interval 1409–1485 (77 years) based only on the regional *Araucaria* chronology, all the other reconstructed segments were based on the PC1 of the regional tree-ring records available for each period. The final reconstructions were developed by integrating the segments for each period of the nested models that passed all the verification tests (Supplementary Table S4). This process was conducted after the mean and the variance of each nested reconstruction segment were adjusted to the

best replicated period (1559–1999), which, in turn, registers the highest r^2 value. This procedure was applied to prevent artificial changes in the variance within the reconstruction due to changes in the variance of the predictors[28]. Two types of error were taken in account to estimate the uncertainties in the SAM reconstructions: the interannual variations in the number and variance of tree-ring series in the regional chronologies (chronology error) and the unexplained variance in the calibration regression model (calibration error)[29].

Full methods and associated references are available in the Supplementary Information.

Received 6 June 2012; accepted 21 September 2012; published online 28 October 2012

References

1. Thompson, D. W. J., Wallace, J. M. & Hegerl, G. C. Annular modes in the extratropical circulation. Part II: Trends. *J. Clim.* **13,** 1018–1036 (2000).
2. Thompson, D. W. J. *et al.* Signatures of the Antarctic ozone hole in Southern Hemisphere surface climate change. *Nature Geosci.* **4,** 741–749 (2011).
3. Polvani, L. M., Waugh, D. J. P., Correa, D. W. & Son, S-W. Stratospheric ozone depletion: The main driver of twentieth-century atmospheric circulation changes in the Southern Hemisphere. *J. Clim.* **24,** 795–812 (2011).
4. McLandress, C. *et al.* Separating the dynamical effects of climate change and ozone depletion. Part II: Southern Hemisphere troposphere. *J. Clim.* **24,** 1850–1868 (2011).
5. Archer, C. & Caldeira, K. Historical trends in the jet streams. *Geophys. Res. Lett.* **35,** L08803 (2008).
6. Hu, Y. & Fu, Q. Observed poleward expansion of the Hadley circulation since 1979. *Atmos. Chem. Phys.* **7,** 5229–5236 (2007).
7. Marshall, G. J. Trends in the southern annular mode from observations and reanalyses. *J. Clim.* **16,** 4134–4143 (2003).
8. Gillett, N. P., Kell, T. D. & Jones, P. D. Regional climate impacts of the Southern Annular Mode. *Geophys. Res. Lett.* **33,** L23704 (2006).
9. Aravena, J. C. & Luckman, B. H. Spatio-temporal rainfall patterns in southern South America. *Int. J. Climatol.* **29,** 2106–2120 (2009).
10. Garreaud, R. D., Vuille, M., Compagnucci, R. & Marengo, J. Present-day South American climate. *Palaeogeogr. Palaeoclimatol. Palaeoecol.* **281,** 180–195 (2009).
11. Watterson, I. G. Components of precipitation and temperature anomalies and change associated with modes of the Southern Hemisphere. *Int. J. Climatol.* **29,** 809–826 (2009).
12. Lara, A., Villalba, R. & Urrutia, R. A 400-year tree-ring record of the Puelo River summer-fall streamflow in the Valdivian Rainforest eco-region, Chile. *Climatic Change* **86,** 331–356 (2008).
13. Boisvenue, C. & Running, S. W. Impacts of climate change on natural forest productivity—evidence since the middle of the 20th century. *Glob. Change Biol.* **12,** 862–882 (2006).
14. Davis, M. B. & Shaw, R. G. Range shifts and adaptive responses to Quaternary climate change. *Science* **292,** 673–679 (2001).
15. Hughes, M. K., Swetnam, T. W. & Diaz, H. F. *Dendroclimatology, Progress and Prospects. Developments in Paleoenvironmental Research 11* (Springer, 2011).
16. Cook, E. R. *et al.* Millennia-long tree-ring records from Tasmania and New Zealand: A basis for modelling climate variability and forcing, past, present and future. *J. Quat. Sci.* **21,** 689–699 (2006).
17. Boninsegna, J. A. *et al.* Dendroclimatological reconstructions in South America: A review. *Palaeogeogr. Palaeoclimatol. Palaeoecol.* **281,** 210–228 (2009).
18. Duncan, R. P., Fenwick, P., Palmer, J. P., McGlone, M. S. & Turney, C. Non-uniform interhemispheric temperature trends over the past 550 years. *Clim. Dynam.* **35,** 1429–1438 (2010).
19. Hendon, H. H., Thompson, D. W. J. & Wheeler, M. C. Australian rainfall and surface temperature variations associated with the Southern Hemisphere Annular Mode. *J. Clim.* **20,** 2452–2467 (2007).
20. Jones, J. M. *et al.* Historical SAM variability. Part I: Century-length seasonal reconstructions. *J. Clim.* **22,** 5319–5345 (2009).
21. Fogt, R. L. *et al.* Historical SAM variability. Part II: Twentieth century variability and trends from reconstructions, observations, and the IPCC AR4 models. *J. Clim.* **22,** 5346–5365 (2009).
22. Karoly, D. J. & Braganza, K. Attribution of recent temperature changes in the Australian region. *J. Clim.* **18,** 457–464 (2004).
23. Masiokas, M. H. *et al.* Glacier fluctuations in extratropical South America during the past 1000 years. *Palaeogeogr. Palaeoclimatol. Palaeoecol.* **281,** 242–268 (2009).
24. Villalba, R. *et al.* Tree-ring based reconstructions of northern Patagonia precipitation since AD 1600. *Holocene* **8,** 659–674 (1998).
25. Lara, A. & Villalba, R. A 3,620-year temperature reconstruction from *Fitzroya cupressoides* tree rings in southern South America. *Science* **260,** 1104–1106 (1993).
26. Cook, E. R., Briffa, K. R., Meko, D. M., Graybill, D. A. & Funkhouser, G. The segment length curse in long tree-ring chronology development for paleoclimatic studies. *Holocene* **5,** 229–237 (1995).
27. Meko, D. M. Dendroclimatic reconstruction with time varying subsets of tree indices. *J. Clim.* **10,** 687–696 (1997).
28. Cook, E. R., Woodhouse, C. A., Eakin, C. M., Meko, D. & Stahle, D. W. Long-term aridity changes in the western United States. *Science* **306,** 1015–1018 (2004).
29. Esper, J. *et al.* Long-term drought severity variations in Morocco. *Geophys. Res. Lett.* **34,** L17702 (2007).
30. Rodionov, S. N. A sequential algorithm for testing climate regime shifts. *Geophys. Res. Lett.* **31,** L09204 (2004).

Acknowledgements

This work was supported by the Inter-American Institute for Global Change Research (IAI) CRN 2047, which is supported by the US National Science Foundation (Grant GEO-0452325), by the Argentinean Council of Research and Technology (CONICET), the Argentinean Agency for Promotion of Science and Technology (PICTR02-186) and by FONDECYT Grant Nos 1090479 and 1120965 from the National Research Fund of Chile. G.J.M. is supported by the UK Natural Environment Research Council through the British Antarctic Survey research programme Polar Science for Planet Earth. K.A. is supported by Australian Research Council grant DP120104320 to P. Baker. This work benefited from discussions with P. Sheppard and A. Bahamondez.

Author contributions

R.V., A.L., M.H.M., R.U., B.H.L. and G.J.M. designed the study, interpreted the data and wrote the paper. J.A.B, G.J.M., D.A., R.N. and A.M.S. assisted with climate data, data analysis and figures. R.V., I.M., M.S.M. and A.M.S. provided tree-ring chronologies for Argentina. A.L., D.A.C., R.U., C.L., J.C.A., E.C. and A.H. provided tree-ring records for Chile. E.R.C., P.F., K.A. and J.G.P. provided tree-ring chronologies for New Zealand and Tasmania. All authors discussed the results and commented jointly on the manuscript.

Additional information

Supplementary information is available in the online version of the paper. Reprints and permissions information is available online at www.nature.com/reprints. Correspondence and requests for materials should be addressed to R.V.

Competing financial interests

The authors declare no competing financial interests.

CLIMATE SCIENCE

Tree rings and storm tracks

Reconstructing past climate in the Southern Hemisphere is a challenge. An analysis of tree-ring records suggests that recent changes in the southern storm track in summer are unprecedented in the past 600 years.

Julie Jones

The influence of the Antarctic ozone hole on surface levels of ultraviolet radiation is well known, particularly to sunbathers in the Southern Hemisphere. Less well known is its role in moving the southern storm track towards the South Pole in summer[1,2]. This large-scale movement of air flow and weather systems has altered surface temperature, precipitation and winds at both mid and high latitudes[3]. As such, it is important to understand how the recovery of Antarctic ozone levels will influence the storm track, and thus surface climate[3]. It is expected that the recovery of the ozone hole and increasing greenhouse gas concentrations will exert strong and opposing influences in the coming decades, with ozone recovery shifting the track towards the Equator, and rising greenhouse gas concentrations shifting it towards the South Pole[3]. Writing in *Nature Geoscience*, Villalba and colleagues[4] show that changes in the Southern Hemisphere storm track in the latter half of the twentieth century significantly modified tree growth, with consequences for climate reconstruction in the region.

Differences in atmospheric pressure between the mid and high latitudes of the Southern Hemisphere are captured by a mode of climate variability known as the Southern Annular Mode (SAM). In the past four decades or so, atmospheric pressure has declined over the South Pole and risen over the mid-latitudes. As a result, the circumpolar westerly winds and the storm track have strengthened. These changes — collectively known as the positive phase of the SAM — have led, for example, to cooling in East Antarctica, and strong warming in parts of the Antarctic Peninsula[3,5]. The latter is thought to have contributed to the collapse of the Larsen B ice shelf in 2002[5].

Records of past changes in the SAM are needed to validate the climate and chemistry-climate models used to project future changes in this mode of climate variability. To date, however, observation-based assessments of SAM behaviour have been restricted to the period of time since 1957, when regular measurements in Antarctica began. These records show a trend towards the positive phase of the SAM since the mid-1960s[5]. Extended reconstructions of the SAM are needed to provide a longer-term perspective.

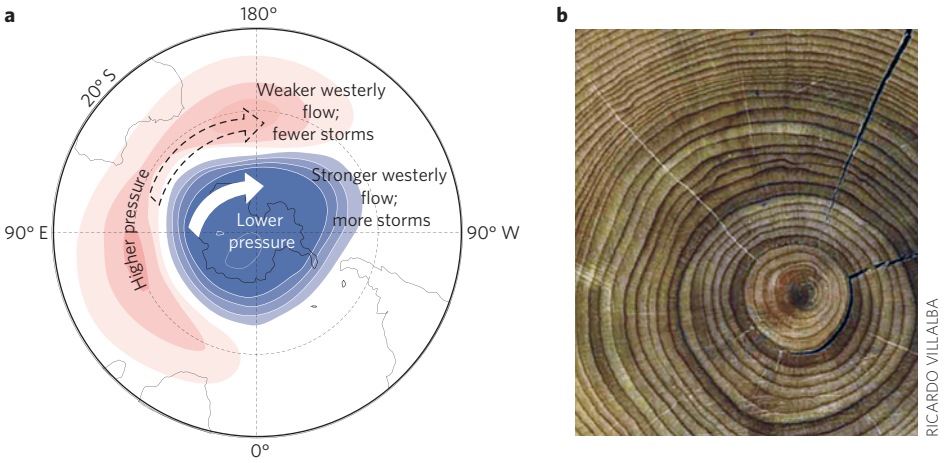

Figure 1 | Positive phase of the Southern Annular Mode. **a**, Differences in atmospheric pressure between the mid and high latitudes of the Southern Hemisphere are captured by a mode of climate variability known as the Southern Annular Mode. The positive phase of this mode, documented here, is characterized by an increase in atmospheric pressure over the mid-latitudes (pink) and a decline in pressure at high latitudes (blue). This pressure difference leads to a strengthening of the circumpolar westerly winds (white arrow) and a southward movement of the Southern Hemisphere storm track. **b**, Villalba and colleagues[4] use tree-ring records to reconstruct changes in the Southern Annual Mode over the past six centuries, and show that it was more positive at the end of the twentieth century than at any other point over this 600-year period.

Villalba and colleagues[4] investigate the influence of ozone-hole-induced changes in the SAM on tree growth over the past few centuries, using tree-ring width data from more than 3,000 trees from Patagonia, New Zealand and Tasmania. They detect a significant shift in tree growth patterns since the 1950s, relative to the previous 250 years, and create regional tree growth records to assess the climatic factors responsible for this shift. According to this approach, the reduction in tree growth in northwestern Patagonia is related to a reduction in summer runoff, and the rise in growth in New Zealand is related to regional warming. These climatic changes, in turn, can be explained by a shift to a more positive phase of the SAM: the higher pressures and weaker westerly winds in the mid-latitudes that accompany the positive phase of the SAM bring fewer moist Pacific air masses, and thus less precipitation, to northwestern Patagonia, and more warm air masses to much of New Zealand[3].

Further exploration of the relationship between tree growth and the SAM, using regression techniques, suggests that variations in SAM behaviour can explain up to 33% and 48% of the variation in tree growth in New Zealand and South America, respectively. On the basis of this relationship, Villalba *et al.* use these tree-ring records to reconstruct changes in the SAM. Their reconstruction extends over the past 600 years, and represents the longest proxy-based record of SAM variability with annual temporal resolution to date. Even when errors are taken into account, the reconstruction suggests that the SAM was more positive at the end of the twentieth century than at any other time over this 600-year period.

This tree-ring-based reconstruction of the SAM supports the results of model simulations and shorter measurement-based records, which also suggest that current values are outside the range of natural variability[6]. Furthermore, Villalba and colleagues demonstrate significant agreement between their reconstructions during the twentieth century and existing ones, giving confidence in their estimates.

Key strengths of their reconstruction of the SAM include the reliance on a large and up-to-date network of trees, the careful analysis of the relationship between tree growth and regional climate, and the production of sound error estimates. The scarcity of tree records extending back to AD 1400 does mean that the earliest parts of the record are based on fewer trees. And as with all reconstructions that rely on relationships between large-scale circulation, local climate and proxies, the assumption is made that these relationships do not change with time. This is difficult to test — if the long time series were available, we would not need reconstructions in the first place. However, it has been suggested that links between SAM and local climate can change through time in some regions[7,8]. This is a particular issue for the Antarctic Peninsula region[7], where the tropical Pacific Ocean modulates the SAM–climate signal, with implications for reconstructions of the SAM reliant on ice-core isotope data from the region.

Villalba and colleagues[4] utilize tree growth signals to show that changes in the summer SAM in the latter half of the twentieth century are unprecedented in the past 600 years. The vast areas of ocean and the inhospitality of Antarctica make reconstructing climate in the Southern Hemisphere a challenging yet fascinating task. Climate reconstructions using new proxy data sources, such as those presented in this study, will help to address this challenge[9]. ❑

Julie Jones is in the Department of Geography, University of Sheffield, Sheffield, S10 2TN, UK.
e-mail: julie.jones@sheffield.ac.uk

References

1. Gillett, N. P. & Thompson, D. W. J. *Science* **302,** 273–275 (2003).
2. Polvani, L. M., Waugh, D. W., Correa, C. J. P. & Son, S. W. *J. Clim.* **24,** 795–812 (2011).
3. Thompson, D. W. J. *et al. Nature Geosci.* **4,** 741–749 (2011).
4. Villalba, R. *et al. Nature Geosci.* http://dx.doi.org/10.1038/ngeo1613 (2012).
5. Marshall, G. J., Orr, A., van Lipzig, N. P. M. & King, J. C. *J. Clim.* **19,** 5388–5404 (2006).
6. Fogt, R. L. *et al. J. Clim.* **22,** 5346–5365 (2009).
7. Marshall, G. J., Di Battista, S., Naik, S. S. & Thamban, M. *Clim. Dynam.* **36,** 277–287 (2011).
8. Silvestri, G. & Vera, C. *J. Clim.* **22,** 6142–6148 (2009).
9. Neukom, R. & Gergis, J. *Holocene* **22,** 501–524 (2012).

Published online: 28 October 2012

nature geoscience
SUPPLEMENTARY INFORMATION
DOI: 10.1038/NGEO1613

Unusual Southern Hemisphere tree growth patterns induced by changes in the Southern Annular Mode

Full Methods

1. Tree-ring records

We examined interannual variations in tree growth during the last centuries from six species growing at mid-latitude forests in the Southern Hemisphere. The database included an updated and expanded network of tree-ring chronologies from South America, Tasmania and New Zealand. The complete list of chronologies showing their geographic location, the period covered by each record, and its source, is included in Supplementary Information Table 1**.** These records included only species with adequate sample replication (>20 trees) through the 1980s and 1990s. In South America, the growth patterns were analyzed for three tree species that are representative of temperate forests, the conifers *Austrocedrus chilensis* (AUCH) and *Araucaria araucana* (ARAR) from dry to mesic sites in North Patagonia, and the evergreen broadleaved *Nothofagus betuloides* (NOBE) from relatively mesic to wet sites in southernmost South America. In Tasmania, we assessed the growth patterns of the conifers *Lagarostrobos franklinii* (LAFR) and *Phyllocladus aspleniifolious* (PHAS). Finally, in New Zealand, tree-ring records of *Halocarpus biformis* (HABI) were studied. Except for LAFR, for which we had access to only three chronologies, the records for the other species included a large number of sites distributed, in most cases, across their geographic range of distribution. Therefore, with exception of the LAFR record, the growth variations shown in this study are fairly representative of the regional patterns of tree growth for each selected species (Fig. 1).

In order to identify the dominant patterns of tree growth at a regional scale for each species, tree-ring chronologies were initially standardized using a cubic spline function designed to reduce 50% of the variance in a sine wave with a periodicity of 150 years[1]. Principal components (PC) were extracted from the records available for each species over the common period AD 1800-1950, which coincides with the interval of highest sample replication for most chronologies. The selection of this period ensures that the signal in each record is representative of the stand growth, reducing the noise associated with low-series replication in the earlier portion of the chronologies. For each species, all records contributing to PC1 with eigenvalues ≥0.60 were combined to develop a regional chronology (Supplementary Information Table 1). This approach was selected as a reasonable compromise between including enough site chronologies to achieve good replication in the regional chronologies while rejecting those chronologies showing site-specific variations due to local fires, logging or insect outbreaks. All the individual series in the regional chronologies were visually

inspected and those exhibiting abrupt changes in growth (releases or suppressions due to stand dynamics) unrelated to climate were removed from the analysis. The use of a relatively lower number of chronologies with a strong internal common signal is the most appropriate method to reduce potential errors associated with the use of larger network of proxy-records that have not been properly assessed for their internal consistency and regional representativeness[2]. Although the three LAFR chronologies had eigenvalues ≥ 0.60 in PC1, only the record from Mount Read was included in the analysis. Previous studies indicated that the records from Lake Marilyn Low and High, located at lower elevations than Mount Read (Supplementary Information Table 1), have different relationships with climate than Mount Read[3,4]. Although represented only by the Mount Read chronology, the LAFR record includes 176 trees and more than 340 series (see Supplementary Information Table 2). For each of the other five species, the regional chronologies included the following number of site chronologies: AUCH: 20 sites; ARAR: 16 sites; NOBE: 4 sites; PHAS: 7 sites; and HABI: 10 sites. The regional chronologies for each species show a wide range of variation in length, number of series, and tree-ring statistics (see Supplementary Information Table 2).

In order to retain the low-frequency signal in each regional chronology, we tested several standardization methods that utilize different curve fittings[5,6]. Standardization aims to remove that part of the variability in tree-ring series not related to climate (e.g., tree aging or forest disturbances). Prior to standardization, variations in the standard deviation associated with changes in the mean tree-ring widths over time were stabilized using a data adaptive power transformation[7]. This power transformation has the advantage of homogenizing the variance in the tree-ring series over their entire length, reducing the heteroscedasticity of the raw tree-ring series. After several trials, we selected two standardization methods to preserve the low-frequency variation in the original tree-ring series (Fig. 1). Individual series from raw chronologies showing an increasing trend during the last decades of the 20th century (Fig. 1, LAFR, PHAS, HABI), were standardized using negative exponential or straight lines with zero or negative slope. In contrast, the decreasing trend in the South American raw chronologies (Fig. 1, AUCH, ARAR, NOBE) was better preserved by standardizing each series with a robust median filter, using a time window of 50% of the individual tree-ring series length. Although this standardization method has rarely been used in previous studies, we found that it is the best available option for recovering the decrease in tree growth during the most recent decades. Different curve fittings for each species are shown in Figures 1 to 6 in the Supplementary Information.

These figures show that depending on the standardization method selected, the patterns in tree growth during the most recent decades can be relatively well maintained or severely modified. Since our purpose was to retain low frequency variation in the records during the 20th century, we

use the standardization method that best reproduced the growth trends recorded in the original (raw) data in the most recent decades. For each selected species, trends in tree growth in the original raw data since AD 1900 and the four chronologies using the standardization methods shown in Supplementary Information Figures 1 to 6 are displayed in Full Methods Figure 1. To facilitate comparisons, all records were normalized over the period 1900-2000. Option 2 (negative exponential curve or linear regression with neg. or zero slope) better captures the positive trends in tree growth recorded in LAFR, PHAS and HABI (New Zealand-Tasmania sites) during the 20th century than other standardization options. The regression coefficients for option 2 are closest to the regression coefficients for the raw data in these chronologies (Full Methods Fig. 1). In contrast, option 4 (median smoothing) provides the best alternative to retain the negative trends in tree growth for AUCH, ARAR and NOBE (South American) chronologies during the past few decades. The regression coefficients for option 4 are closest to those recorded in the raw data from these chronologies. Interestingly, none of the selected standardization options spuriously inflate or exacerbate the trends in the raw data in the 20th century. As shown in Full Methods Figure 1, trends in the standardized chronologies are lower (in absolute values) than those in the raw data.

Although increases in chronology mean ages could be invoked as a possible cause for the persistent reduction in tree growth during recent decades in the South American records, the same reasoning is not valid for the Tasmanian-New Zealand chronologies showing similar trends in mean ages as the South American records but opposite patterns in radial growth (Full Methods Fig. 2). As clearly shown in Figure 2, the anomalous patterns in tree growth recorded over most recent decades are consistent with the climate changes recorded at regional scales, which in South America and New Zealand are tightly associated with the persistent trends in the summer SAM since the 1950's. In addition, the mean segment length of the six regional chronologies at the end of the 20th century ranges between 234 and 468 years (Full Methods Fig. 2), suggesting that these segment lengths have little effect on the growth signal on time scales of 2 to 4 decades or even longer.

Multi-decadal shifts in mean conditions in the regional raw chronologies were identified using a simple regime shift detection technique[8,9] with a cut-off segment length l = 20 years, a target probability level p = 0.05, and an outlier weighting factor h = 2 (Fig. 1). In order to ensure that the identified shifts are not simply the manifestation of a red noise process, each series was prewhitened prior to testing (see references 8 and 9 for further details on this methodology).

2. Climate-tree growth relationships

In order to identify the climate drivers at hemispheric or continental scales associated with the variations in radial tree growth of temperate forests in the Southern Hemisphere, the standardized chro-

nologies were compared with tropical and extra-tropical circulation indices including the Southern Oscillation Index (SOI) and the Southern Annular Mode (SAM) index. The correlation coefficients between the six regional chronologies and the seasonal SAM-Marshall[10] and SAM-NCEP[11] indices for the Southern Hemisphere summer (DJF) are shown in Supplementary Information Table 3. In addition, correlation coefficients between the chronologies and the SOI in summer (DJF), autumn (MAM), winter (JJA) and spring (SON) are included. The dominant pattern involves significant correlations between the regional chronologies and the summer SAM index. These are generally negative for the South American species and positive for species from Tasmania and New Zealand. Since the marked trend in the SAM instrumental records (increasing) and the tree-ring chronologies (increasing or decreasing) during the recent decades might inflate the statistical significance of the correlation between records, the long-term trends were removed by using regression techniques for the SAM indices and autoregressive processes for the tree-ring records[12]. Correlation coefficients remained significant between the SAM indices and the AUCH, ARAR, NOBE and HABI regional chronologies during summer (DJF, Supplementary Information Table 3) even after accounting for linear trends/autocorrelation in the series, a clear indication of consistent relationships between summer SAM variations and tree-growth. Although significantly correlated with the SAM-Marshall index over the 1957-2007 interval, the NOBE regional chronology has a weaker relationship with the SAM-NCEP index over the 1948-2004 period. The LAFR and PHAS regional chronologies are not significantly correlated with the summer SAM indices once the long-term trends are eliminated (Supplementary Information Table 3).

In addition to testing the strength of the relationships between the SAM and regional tree growth, we also assessed the relationships between (1) the SAM index and the hydro-climate of the regions where the selected species grow, and (2) the regional tree growth and those hydroclimatic parameters affected by the SAM. Our intention here was to show that (1) the SAM influences the hydroclimate in the selected areas and (2) the radial growth of the species of interest is effectively connected with those climate variables affected by the SAM.

In addition, we aim to provide a measure of the percentage of tree growth directly related to the SAM index for each species. Since our previous analyses of the relationships between the SAM index and tree growth (Supplementary Information Table 3) suggested that the strongest relationships occur in summer, the SAM and regional climate conditions were evaluated during the months of December, January and February, or a combination of them. For some species, spring and fall conditions were also included in seasonal means of the SAM, streamflows or temperatures in addition to summer months. As tree growth is commonly influenced by climate during the current and the previous growing seasons[13], climate and the SAM index during the previous growing season

were also considered in determining the strongest relationships between tree growth, regional climate, and the SAM. For example, the streamflow of the Río Chubut in December-January is clearly modulated by the SAM conditions during these two months (r = -0.54; Fig. 2a). The streamflow variations of Río Chubut during the previous and current growing seasons (January to March), an integrative measure of moisture in the dry eastern slopes of the Andes, explain almost 50% of the total variance in AUCH tree growth over the interval 1945-2005 (r = 0.70). Finally, the SAM in January of the previous growing season in combination with the SAM index in summer (DJF) of the current growing season explain from 27% up to 44% of the total variations in AUCH tree growth during the common period 1957-2003 (Fig. 2m). A similar analysis indicated that (1) the SAM in summer and fall (December to May) modulated 37 to 42% of the total variations in the Río Cautín streamflows during the past 47 years (Fig. 2b), (2) summer-fall variations of the Río Cautín during previous and current growing seasons are closely related to ARAR tree growth (Fig. 2h), and (3) the SAM in previous January and current January to March explain between 20 and 38% of the total variance in ARAR tree growth since the year 1957 (Fig. 2n). In establishing the range of total variance in radial growth explained by SAM we followed the Marshall et al. (2006) approach[14], using correlations between detrended and non-detrended data to provide estimations of the minimum and maximum percentages in tree growth variations modulated by the SAM, respectively. Consistent with the results shown in Supplementary Information Table 3, our complementary analyses show that the influence of the SAM on regional climates is stronger in northern Patagonia (Fig. 2a and b) and New Zealand (Fig. 2f) than in southern Patagonia (Fig. 2c) and Tasmania (Figs.2 d and e). Unfortunately, the lack of reliable precipitation records hinders the precise determination of the SAM influences in southern Patagonian climate. The low correlation coefficient between the SAM index and summer temperatures in Tasmania is consistent with recent studies suggesting a weaker influence of the SAM on Tasmanian temperature[15]. According to these results, the total variation in tree growth explained by the SAM index in summer reached maximum values around or above 40% in the South American forests and 33% in the New Zealand forests. In contrast, the growth of LAFR and PHAS, which are highly correlated with local temperatures in summer-fall and winter-spring, respectively (Figs. 2 j and k), were poorly associated with the SAM index (maximum percentages between 12 and 17%; Figs. 2 p and q).

All of the regional chronologies, except for PHAS, were significantly correlated with instrumental-based SAM reconstructions starting in 1866[16,17] (Supplementary Information Table 3). However, consistent with our previous analyses, the regional chronologies from northern Patagonia and New Zealand show the stronger associations with the instrumental-based SAM reconstructions. Given the weaker correlations of PHAS and LRFR chronologies with the instrumental SAM-Marshall and

SAM-NCEP records, and that between NOBE and SAM-NCEP index, these records were not included as predictors of the SAM indices in the tree-ring based reconstructions discussed below. In addition, these four regional chronologies show weaker correlations with the instrumental-based SAM reconstructions than the AUCH, ARAR and HABI chronologies (Supplementary Information Table 3).

3. Tree-ring based SAM reconstructions

Based on our previous analysis, the AUCH, ARAR and HABI chronologies were selected as potential predictors for the SAM index reconstructions. The first principal component (PC1) from the AUCH, ARAR and HABI regional chronologies captured 60% of the total variations in tree growth during the common period 1559-1999 (441 years) and was significantly correlated with the summer SAM instrumental variations. The interval 1599-1999 had good replication with ≥30 series in each regional chronology (Fig. 1 and Supplementary Information Table 1). The contribution of each regional chronology to PC1 loadings was higher for the South America (-0.80 and -0.82 for AUCH and ARAR, respectively) than for the New Zealand region (0.69 for HABI), reflecting the highly significant correlation between the two South American records ($r = 0.514$, n = 441, $p<0.001$). The association between this common pattern of tree growth (PC1) in temperate forests of the SH and the summer SAM is highly consistent even using different SAM records. This is valid for the SAM index derived from (a) a selection of pressure station records from mid and high latitudes of the Southern Hemisphere (SAM-Marshall[10], $r = 0.67$, n = 43), (b) the mean sea-level pressure south of 20°S (SAM-NCEP[11], $r = 0.70$, n = 52), as well as from (c) reconstructions based on longer pressure records from stations at mid-latitudes in the Southern Hemisphere (SAM-Fogt[16], $r = 0.45$, n = 135, and SAM-Jones[17], $r = 0.44$, n = 135). Note that while the early NCEP reanalysis data are poor over high southern latitudes the errors are smallest during summer, although the seasonal trend is 50% higher than in observations[10].

In order to maximize the length of the SAM reconstructions, we used a nested regression approach in which the shortest predictor series (i.e. the regional tree-ring chronology covering the shortest time interval) was progressively excluded from the regression analyses, and the regression procedure repeated again utilizing the remaining, longer regional chronologies[18,19]. This reconstruction technique enables the use of concatenated PC records to provide longer reconstructions not limited by the shortest record in the set of predictors. Statistics of SAM-Marshall and SAM-NCEP reconstructions are included in Supplementary Information Table 4. In order to develop the nested reconstructions, the PC1 in year *t* (i.e. without lagging the series) of the following chronologies was used for the intervals indicated in parentheses: AUCH, ARAR, and HABI (1559-1999) and ARAR

and HABI (1486-1558). The SAM reconstruction during the interval 1409-1485 is solely based on the ARAR regional chronology. For the reconstruction of the interval 2000-2003, we used the PC1 from the two South American chronologies (AUCH and ARAR) since the record from New Zealand was not available for this period. The most recent three years (2004-2006) were estimated using the ARAR regional chronology. The regression model based on the PC1 which includes the three regional chronologies explains 47.4 % and 43.6% of the total variance in the SAM-NCEP (1948-1999) and SAM-Marshall (1957-1999) records, respectively. As expected, the percentage of explained variance decreases back in time as the number of chronologies used to generate the PC predictors decreases, reaching 29.1 % and 24.0% of the explained variance for the SAM-NCEP and SAM-Marshall records, respectively, when only the ARAR chronology is used as predictor (Supplementary Information Table 4). All regression models were cross-validated using a leave-one-out approach[18].

Two types of error were considered in establishing the uncertainties in the SAM reconstructions. These errors included the uncertainties related to changes in the number and variance of regional chronologies back in time (chronology error) and the uncertainty due to unexplained variance in the regression models (calibration error) [20,21].

Interannual variations in the standard error of the chronology (S_c), a statistic accounting for both the dispersion around the mean and the varying number of the ring-with measurements per year, was used to quantify the year-to-year variations the chronology error[13] (Full Methods Fig. 3). Interannual variations in the S_c of the regional chronologies were transferred to the SAM reconstructions weighting the S_c values by the PC loadings of each chronology in the PC1 used as predictor of the SAM indexes. In the nested SAM index reconstructions, the combined or single S_c associated with the PC1s and the ARAR chronology, respectively, were scaled using the slope regression coefficients from the calibration equations between the PC1 and the SAM instrumental indices.

In addition, three different statistics used to estimate the calibration error in the SAM reconstructions were computed: (1) the standard error of the estimate (S_e), (2) the root-mean-squared error of validation (RMSE*v*) and the standard deviation of the residuals (SD*res*) in the calibration models[20-22]. The chronology and calibration errors were quantified separately (Full Methods Fig. 4) and combined (Full Methods Fig. 5) to provide an appreciation of the total errors related to nested SAM-index reconstructions. Due to the extremely high replication in the regional chronologies over the intervals used in the SAM reconstructions (mean replication of 413 samples over the period 1558-2003 for AUCH, 324 samples over the period 1408-2006 for ARAR and 273 samples for HABI over the period 1485-1999), the chronology errors are lower than the calibration errors (Full Methods Fig. 4). The combined uncertainty was estimated from the square root of the summed and

squared chronology and calibration errors[20]. The integration of the chronology error with the calibration error based on RMSE*v* provides the most conservative estimates for the SAM reconstructions (Full Methods Fig. 5). This error combination is displayed in Figure 4 for both the SAM-Marshall and SAM-NCEP index reconstructions.

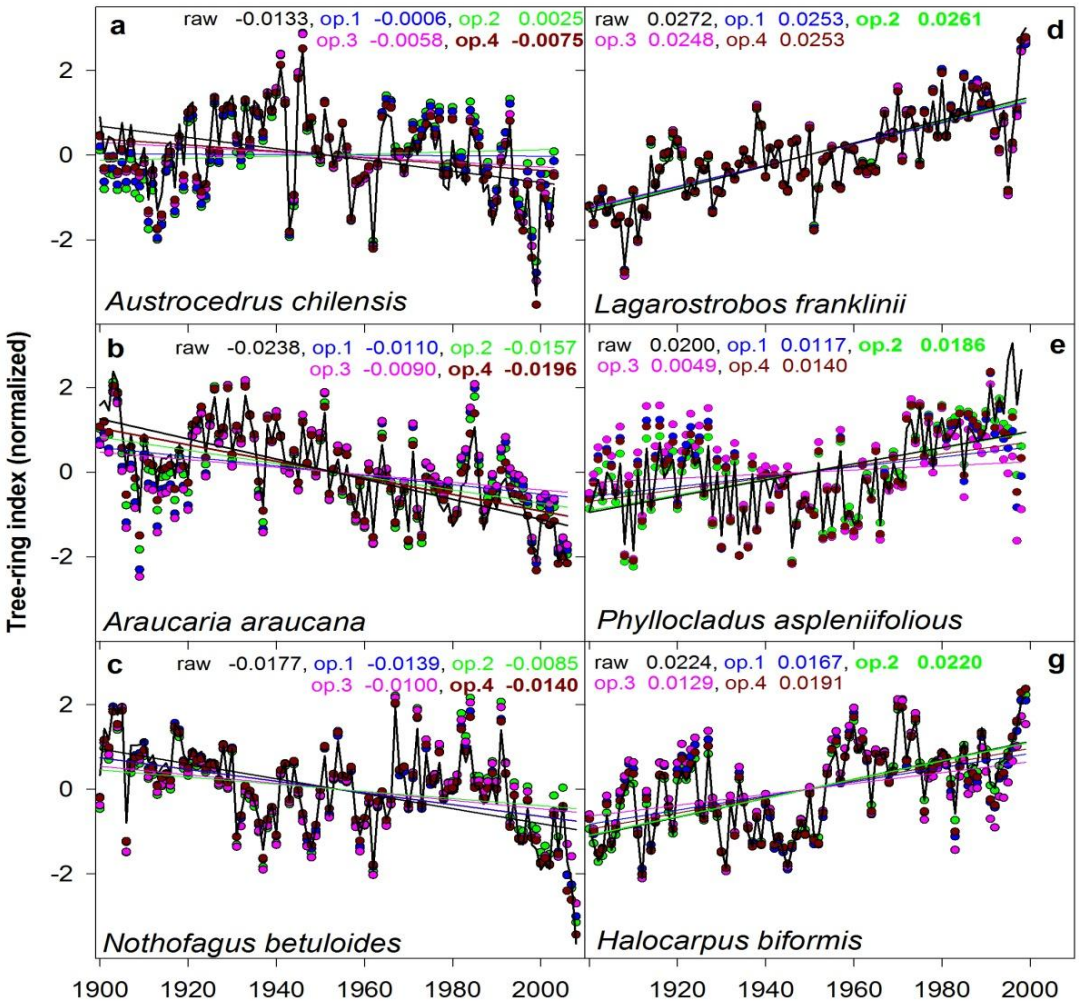

FM_Figure 1. Comparison of normalized tree-growth regression trends during the 20th century between the raw chronologies (solid black line) and the chronologies standardized using four different options. Op. 1 (blue): negative exponential curve or linear regression (any slope); Op. 2 (green): negative exponential curve or linear regression (neg. or zero slope); Op. 3 (pink): general negative exponential curve; Op. 4 (brown): median smoothing. For each species, the regression coefficients are indicated for the raw and the four standardized chronologies. For the South American chronologies (a, b and c), the standardization using median smoothing provides the regression trends closer to those recorded in the raw chronologies. In contrast, the standardization using negative exponential curves or linear regressions with negative or zero slopes show linear trends closer to the raw data for the Tasmania (d and e) and New Zealand (f) chronologies. Note that none of the standardization methods used exacerbates the trends in the raw data.

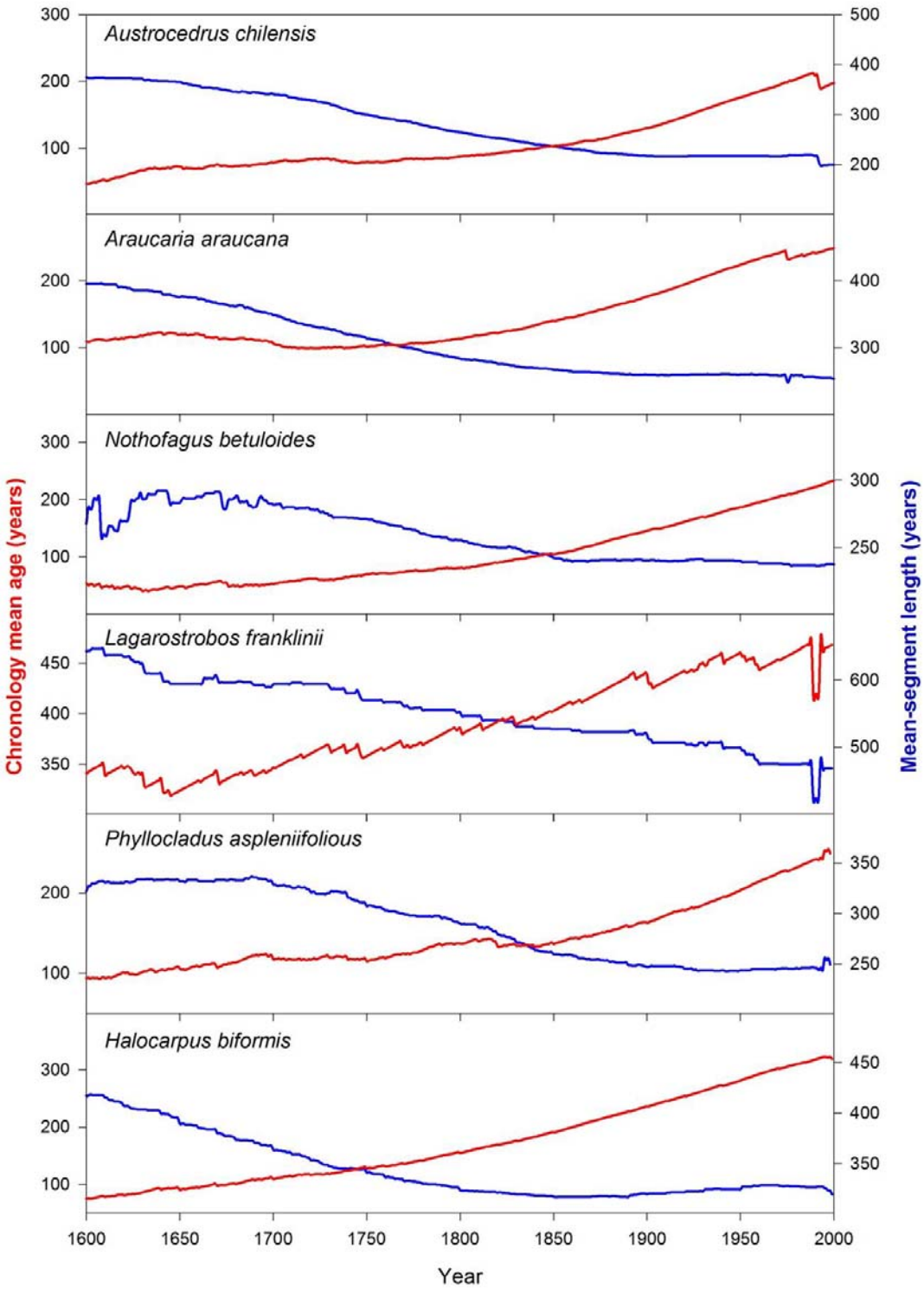

FM_Figure 2. Patterns of mean age (red) and segment-length (blue) for the tree-ring chronologies used in this study. Note the similarities in both patterns between the different chronologies.

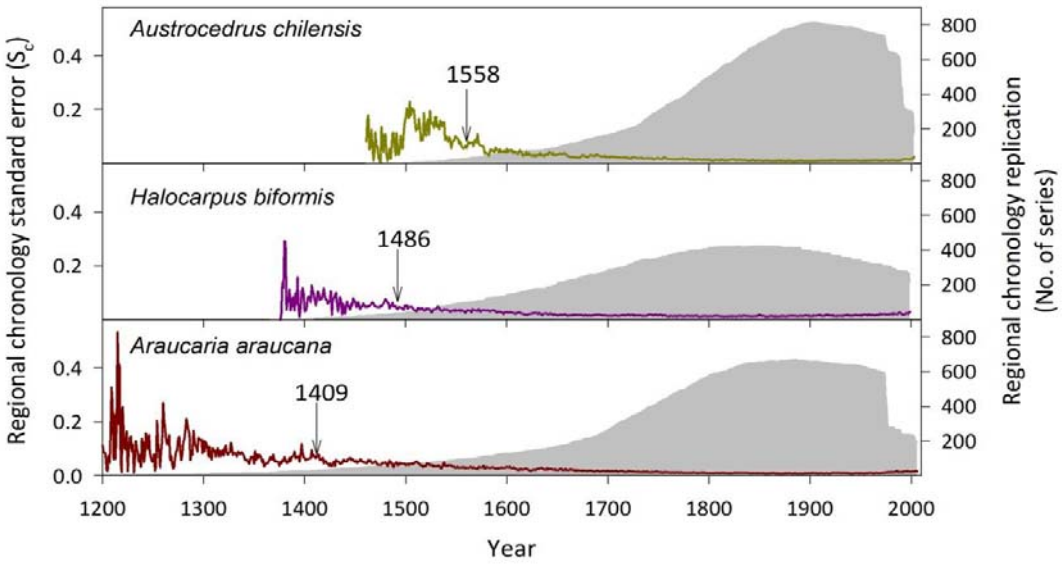

FM_Figure 3. Temporal variations in regional chronology errors (standard error of the chronology, S_c) related to the varying number of ring with measurements back in time and variance of the series around the mean tree-ring index in each chronology. Grey areas represent the replication curves for each regional chronology. Arrows indicate the first year in each chronology with replication ≥ 30 series. We used this criterion to establish the chronology period suitable for developing the reconstructions (more severe than EPS ≥ 0.85).

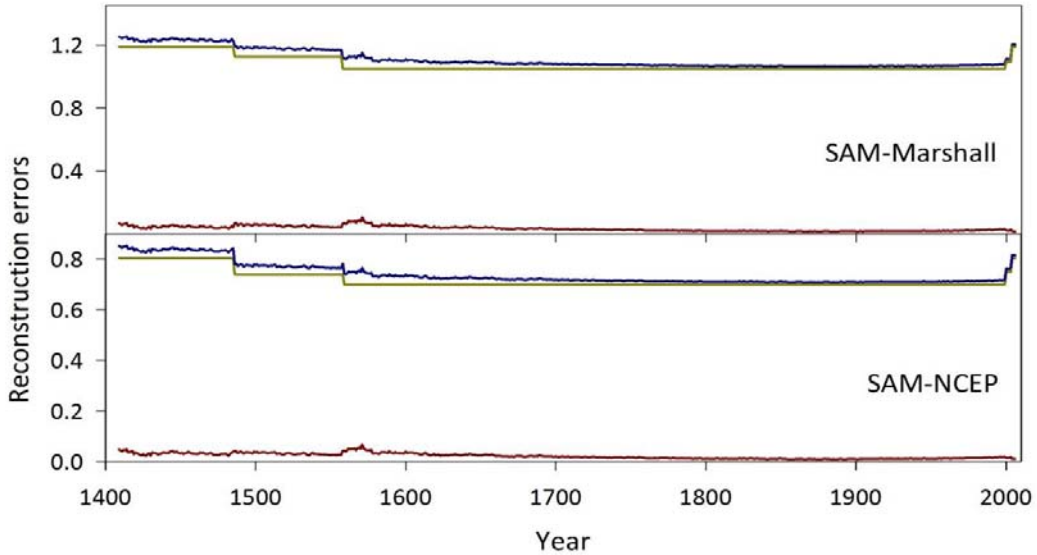

FM_Figure 4. Total uncertainties in the SAM-Marshall and SAM-NCEP reconstructions resulting from the sum (blue line) of interannual changes in the number and variance of ring width series around the mean annual ring indices in the regional chronologies (integrated standard error of the chronology S_c; dark red line) and the unexplained variance in the regression model derived from calibration of the PC1 of the regional chronologies (AUCH, ARAR, HABI over the period 1559-1999; ARAR and HABI over the period 1486-1558; AUCH-ARAR over the years 2000-2003) and the ARAR regional chronology (1409-1487; 2004-2006) against the summer SAM-Marshall and

SAM-NCEP indices (calibration error RMSE*v*; dark green line). The integration of the chronology and calibration errors provides an estimation of the overall errors for the nested SAM-index reconstructions.

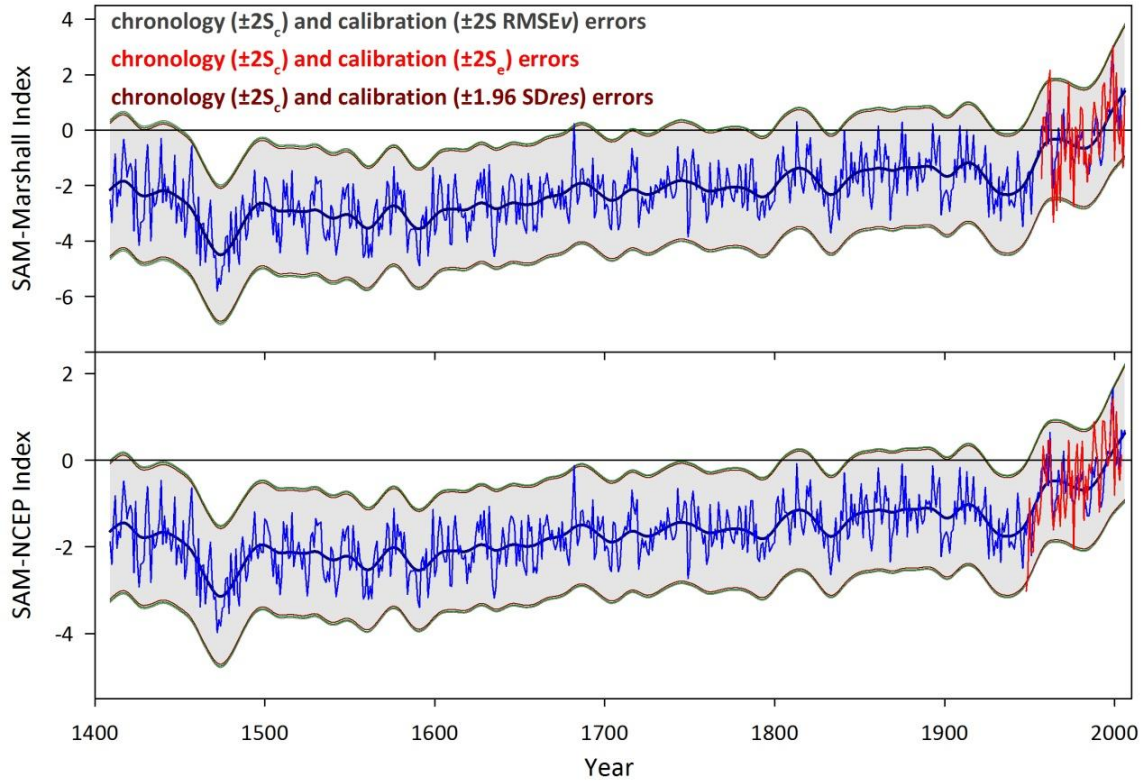

FM_Figure 5. Summer SAM-Marshall and SAM-NCEP index reconstructions (thin blue lines) together with the 30-year smoothed (thick blue lines) versions back to 1409. Bands around the reconstructions display the errors resulting from the integration of the chronology (±2S$_c$) and calibration uncertainties based on the standard error of estimate (±2S$_e$), the root-mean squared error of validation (±2RMSE*v*) and the standard deviations of the calibration residuals (±1.96 SD*res*). The three error bands look virtually identical. All error bands smoothed with a 30-year spline filter. Red lines are the instrumental SAM-Marshall and SAM-NCEP indices during austral summer (December to February). Both, the SAM-Marshall and SAM-NCEP indices are dimensionless.

Full Method References

1. Cook, E.R. & Peters, K. The smoothing spline: a new approach standardizing forest interior tree-ring series for dendroclimatical studies. *Tree-Ring Bull.* **41**, 45-53 (1981).
2. Frank, D., Esper, J., Zorita, E. & Wilson, R. A noodle, hockey stick, and spaghetti plate: a perspective on high-resolution paleoclimatology. WIREs *Clim. Change* **1**, 507-516 (2010).

3. Buckley, B.M., Cook, E.R., Peterson, M.J. & Barbetti, M. A changing temperature response with elevation for *Lagarostrobos franklinii* in Tasmania, Australia. *Clim. Change* **36,** 477-498 (1997)

4. Cook, E.R. et al. Millennia-long tree-ring records from Tasmania and New Zealand: A basis for modelling climate variability and forcing, past, present and future. *J. Quaternary Sci.* **21**, 689-699 (2006).

5. Cook, E.R. A time series analysis approach to tree ring standardization. PhD. Dissertation, University of Arizonan Tucson, 185 pp. (1985).

6. Briffa, K., & Melvin, T.M. in: *Dendroclimatology, Progress and Prospects. Developments in Paleoenvironmental Research* (eds Hughes, M.K., Swetnam, T.W. & Diaz, H.F.) 113-145 (Springer, Dordrecht, 2011)

7.Cook, E.R. & Peters, K. Calculating unbiased tree-ring indices for the study of climatic and environmental change. *The Holocene* **7**, 361-370 (1997).

8. Rodionov, S.N. A sequential algorithm for testing climate regime shifts. *Geophys. Res. Lett.* **31**, doi: 10.1029/ 2004GL019448 (2004).

9. Rodionov, S.N. The use of prewhitening in climate regime shift detection. *Geophys. Res. Lett.,* **33**, L12707, doi:101029/2006GL025904 (2006).

10. Marshall, G. J. Trends in the southern annular mode from observations and reanalyses. *J. Climate*, **16**, 4134-4143 (2003).

11. Thompson, D. W. J. & Wallace, J. M. Annular modes in the extratropical circulation. Part I: Month-to-month variability. *J. Climate,* **13,** 1000-1016 (2000).

12. Cook, E.R. The decomposition of tree-ring series for environmental studies. *Tree-Ring Bull.* **41**, 45-53 (1987).

13. Fritts, H. *Tree Rings and Climate* (Academic Press, New York, 1976).

14. Marshall, G.J., Orr, A., van Lipzig, N.P.M. & King, J.C. The impact of a changing Southern Hemisphere annular mode on Antarctic Peninsula summer temperatures. *J. Climate*, **19**, 5388-5404 (2006).

15. Hendon, H. H., Thompson, D.W.J. & Wheeler, M.C. Australian rainfall and surface temperature variations associated with the Southern Hemisphere Annular Mode. *J. Climate*, **20**, 2452-2467 (2007).

16. Fogt, R. L. et al. Historical SAM variability. Part II: Twentieth century variability and trends from reconstructions, observations, and the IPCC AR4 models. *J. Climate*, **22**, 5346-5365 (2009).

17. Jones, J. M. et al. Historical SAM variability. Part I: Century-length seasonal reconstructions. *J. Climate* **22**, 5319-5345 (2009).

18. Meko, D.M. Dendroclimatic reconstruction with time varying subsets of tree indices. *J. Climate* **10**, 687-696 (1997).
19. Cook, E.R., Woodhouse, C.A., Eakin, C.M., Meko, D. & Stahle, D.W. Long-term aridity changes in the western United States. *Science* **306**, 1015-1018 (2004).
20. Esper J. et al. Long-term drought severity variations in Morocco. *Geophys. Res. Lett.* **34**, L17702, doi: 17710.11029/ 12007gl030844 (2007).
21. Esper, J. et al. 2012. Orbital forcing of tree-ring data. *Nature Climate Change*, DOI: 10.1038/NCLIMATE1589.
22. Jones, J. M., & Widmann, M. Instrument and tree-ring estimates of the Antarctic Oscillation. *J. Climate* **16**, 3511–3524 (2003).

Supplementary Information

SI_Table 1. Tree-ring chronologies considered in this study. Only chronologies with eigenvalues ≥ 0.6 in the first principal component (PC1 eigenv.) for the period 1800-1950 (shown in bold red), were included in the regional chronology for each species.

Species/Sites	Code	Latitude/Longitude	Elev. (m)	Period	No. of radii	No. of trees	PC1 eigenv.	Source
Austrocedrus chilensis								
El Asiento	ELA	32°39'S/ 70°49'W	1800	955-2000	114	94	0.09	LaMarche et al. (1979)[1] ,updated
San Gabriel	CH007	33°47'S/ 70°15'W	1600	1131-1975	63	63	0.22	LaMarche et al. (1979)[1]
Río Clarillo	RCL	33°49'S/ 70°25'W	1900	1204-2002	80	40	0.05	Le Quesne et al. (2009)[2]
El Baule	ELB	34°29'S/ 70°26'W	1850	1146-2001	49	34	0.12	Le Quesne et al. (2009)[2]
Agua de la Muerte	AMU	34°31'S/ 70°25'W	1850	1072-2001	108	57	0.12	Le Quesne et al. (2009)[2]
Santa Isabel	CH013	34°47'S/ 70°45'W	850	1613-1975	64	64	0.26	LaMarche et al. (1979)[1]
Alto las Mesas	CH001	34°54'S/ 70°42'W	1020	1823-1975	7	7	0.04	LaMarche et al. (1979)[1]
Melado	CAC	35°52'S/ 71°00'W	1435	1270-2005	108	59	0.33	Christie et al. (2011)[3]
Polcura	POL	37°04'S/ 71°24'W	1205	1144-2004	154	88	0.36	Christie et al. (2011)[3]
Huinganco	HUI	37°07'S/ 70°36'W	1450	190-2000	162	104	0.43	LaMarche et al. (1979)[1], updated
El Chacay	CH011	37°21'S/ 71°03'W	925	1641-1975	16	16	0.52	LaMarche et al. (1979)[1]
Abanico	CH010	37°21'S/ 71°35'W	820	1733-1975	25	25	**0.64**	LaMarche et al. (1979)[1]
Nitrao	NIT	37°41'S/ 71°17'W	1220	1339-2005	119	58	0.48	Christie et al. (2011)[3]
Ralco-Lepoy	RAL	38°03'S/ 71°18'W	1080	1585-2005	88	60	0.59	Christie et al. (2011)[3]
Ñorquinco	NOR	39°07'S/ 71°07'W	1150	1562-2003	102	52	**0.69**	Villalba et al. (1998)[4], updated
Rucachoroi	RUC	39°15'S/ 71°10'W	1300	1572-2003	50	40	**0.74**	LaMarche et al. (1979)[1], updated
Quillén	QUI	39°17'S/ 71°16'W	1100	1676-1989	19	13	0.54	Villalba et al. (1998)[4]
Collun-co Alto	COL	39°56'S/ 71°08'W	870	1596-1989	18	12	**0.66**	Villalba et al. (1998)[4]
Cerro La Hormiga	HOR	40°03'S/ 71°17'W	920	1508-2003	61	36	**0.83**	Villalba et al. (1998)[4], updated
Cerro Los Pinos	PIN	40°04'S/ 71°02'W	1100	1508-2003	67	44	**0.62**	Villalba et al. (1998)[4], updated
Cerro Castillo	CAS	40°31'S/ 71°09'W	1070	1576-2003	32	17	**0.72**	Villalba et al. (1998)[4], updated
El Mirador	MIR	40°39'S/ 71°24'W	1050	1484-2003	52	28	**0.81**	Villalba et al. (1998)[4], updated
Piedra del Viento	VIE	40°42'S/ 71°08'W	910	1679-1991	14	7	0.57	Villalba et al. (1998)[4]
Arroyo Minero	MIN	40°42'S/ 71°16'W	1050	1589-1991	16	10	**0.71**	Villalba et al. (1998)[4]
Confluencia Traful	CF2	40°42'S/ 71°09'W	1075	1723-1989	24	22	**0.78**	Villalba et al. (1998)[4]
Cuyín Manzano	CUY	40°43'S/ 71°08'W	900	1543-2003	39	27	**0.81**	LaMarche et al. (1979)[1], updated
El Centinela	CEN	40°44'S/ 71°06'W	1050	1489-2002	43	27	**0.85**	Villalba et al. (1998)[4], updated
Dedo de Dios	DDD	40°44'S/ 71°06'W	900	1461-1989	37	24	**0.83**	Villalba et al. (1998)[4]
Cerro El Guanaco	GUA	41°02'S/ 70°59'W	1150	1497-2002	36	22	**0.81**	Villalba et al. (1998)[4], updated
San Ramón	RAM	41°03'S/ 70°59'W	1100	1650-1991	17	10	**0.75**	Villalba et al. (1998)[4]
Cerro Los Leones	LEO	41°05'S/ 71°09'W	1020	1539-2003	73	53	**0.86**	LaMarche et al. (1979)[1], Villalba et al. (1998)[4], updated
Pilcaniyeu	PIL	41°11'S/ 70°45'W	1100	1733-1991	14	7	**0.72**	Villalba et al. (1998)[4]
P. del Toro	PAM	41°32'S/ 71°29'W	1160	1741-1991	15	15	**0.65**	Villalba et al. (1998)[4]

La Fragua	FRA	41°06'S/ 70°54'W	1180	1690-2002	23	12	**0.64**	Lab. de Dendrocronología-UACH
El Maitén	MAI	41°59'S/ 71°15'W	710	1690-1974	13	13	0.35	LaMarche et al. (1979)[1]
Estancia Teresa	TER	42°57'S/ 71°14'W	820	1540-2002	39	34	0.52	LaMarche et al. (1979)[1], Villalba et al. (1998)[4], updated
Nahuel-Pan	NAU	42°58'S/ 71°13'W	850	1567-2002	84	49	0.58	Villalba et al. (1998)[4], updated
L. Terraplén	RRA	43°01'S/ 71°34'W	650	1700-1974	23	23	**0.62**	LaMarche et al. (1979)[1]
Futaleufú	FUT	43°11'S/ 71°42'W	470	1700-1992	16	8	0.28	Villalba et al. (1998)[4]
Araucaria araucana								
Caramávida	CAR	37°40'S/ 73°10'W	900	1474-1975	21	7	0.24	LaMarche et al. (1979)[1]
Copahue	COP	37°48'S/ 71°04'W	1720	1640-1974	10	5	**0.71**	LaMarche et al. (1979)[1]
Piedra del Águila	PIE	37°49'S/73°01'W	1300	1239-1975	35	12	0.51	LaMarche et al. (1979)[1]
Caviahue	CAV2	37°50'S/ 71°01'W	1685	1444-2003	58	35	**0.80**	LaMarche et al. (1979)[1], Mundo et al. (2011)[5]
Ralco	RAL1	37°55'S/ 71°22'W	1280	1592-2006	26	15	0.10	Lab. de Dendrocronología-UACH
Vizcacha	VIZ1	37°57'S/ 71°17'W	1440	1673-2006	24	23	0.58	Lab. de Dendrocronología-UACH
Chenque Pehuén	CHE	38°06'S/ 70°51'W	1616	1246-1974	42	18	**0.75**	LaMarche et al. (1979)[1]
Nalcas	NAL	38°19'S/ 71°20'W	1420	1386-1975	28	8	**0.66**	LaMarche et al. (1979)[1]
Volcán Lonquimay	LOQ	38°19'S/ 71°34'W	1510	1664-1975	53	15	**0.67**	LaMarche et al. (1979)[1]
Coloradito	COL1	38°25'S/ 71°35'W	1300	1612-2006	29	29	0.04	Lab. de Dendrocronología-UACH
Colorado	COLO	38°25'S/ 71°32'W	1400	1607-2006	14	10	0.01	Lab. de Dendrocronología-UACH
Pino Hachado	HAC2	38°40'S/ 70°50'W	1622	1424-2006	65	36	**0.80**	LaMarche et al. (1979)[1], Mundo et al. (2011)[5]
Paso del Arco	PAR	38°49'S/ 71°04'W	1697	1264-2006	36	19	0.40	Mundo et al. (2011)[5]
P. Pinos Aluminé	PRI	38°52'S/ 70°37'W	1620	1140-1974	28	11	**0.76**	LaMarche et al. (1979)[1]
Lonco Luan	LON	38°59'S/ 71°03'W	1164	1306-1974	41	15	**0.71**	LaMarche et al. (1979)[1]
Remeco	REM	39°05'S/ 71°19'W	1217	1450-2006	40	24	0.59	Mundo et al. (2011)[5]
Ñorquinco	NOR	39°09'S/ 71°14'W	1142	1676-2006	46	27	**0.65**	Mundo et al. (2011)[5]
Estancia Pulmarí	PUL	39°09'S/ 71°13'W	1181	1589-1989	28	15	**0.68**	Villalba et al. (1989)[6]
Lago Rucachoroi	RUC2	39°13'S/ 71°09'W	1317	1377-2006	130	53	**0.81**	LaMarche et al. (1979)[1], Mundo et al. (2011)[5]
Pinalada Redonda	PINA	39°19'S/ 71°17'W	1119	1606-2006	41	25	0.57	Mundo et al. (2011)[5]
Rahue	RAH2	39°23'S/ 70°47'W	1455	1483-2006	65	35	**0.76**	LaMarche et al. (1979)[1], Mundo et al. (2011)[5]
Ea. Nahuel Mapi	MAP	39°32'S/ 71°02'W	1531	1525-2006	44	25	**0.86**	Mundo et al. (2011)[5]
Paso Tromen	TRO2	39°36'S/ 71°25'W	1222	1385-1983	22	12	**0.75**	Villalba et al. (1989)[6]
Lago Tromen	TRO	39°37'S/ 71°20'W	965	1617-1976	49	18	**0.68**	LaMarche et al. (1979)[1]
Volcán Lanín	LAN	39°36'S/ 71°26'W	1565	1291-2006	47	26	**0.81**	Mundo et al. (2011)[5]
Ea Mamuil-Malal	MAM	39°40'S/ 71°13'W	890	1689-1976	26	10	0.52	LaMarche et al. (1979)[1]
Nothofagus betuloides								
Beatriz B1	BEA1	53°43'S/ 72°29'W	45	1812-2008	31	31	0.23	CEQUA
Alejandro A0	ALE0	53°44S/ 72°28'W	19	1704-2008	30	30	-0.24	CEQUA
Alejandro A2	ALE2	53°44'S/ 72°28'W	23	1802-2008	23	23	-0.39	CEQUA
P. L. Despreciado	LDP	54°20'S/ 68°49'W	401	1624-2005	66	55	**0.84**	Lab. de Dendrocronología-UACH
Lago Deseado L.N.	LDN	54°22'S/ 68°46'W	455	1527-2005	52	25	**0.78**	Lab. de Dendrocronología-UACH
Lago Fagnano 1	LFA	54°28'S/ 68°41'W	310	1577-2005	59	25	**0.78**	Lab. de Dendrocronología-UACH

Bahía Crossley	AR031	54°42'S/ 64°39'W	20	1715-1986	15	10	0.11	Boninsegna et al. (1989)[7]
Bahía B. Suceso	AR026	54°49'S/ 65°12'W	35	1751-1986	15	11	0.18	Boninsegna et al. (1989)[7]
Bahía York	AR024	54°49'S/ 64°19'W	60	1647-1986	31	26	0.15	Boninsegna et al. (1989)[7]
Puerto Parry	AR051	54°49'S/ 64°21'W	20	1726-1986	23	14	0.25	Boninsegna et al. (1989)[7]
Río Moat	MOA	54°53'S/ 66°54'W	50	1528-1986	24	13	0.47	Boninsegna et al. (1989)[7]
Ea. Haberton	AR040	54°54'S/ 67°19'W	30	1700-1985	23	17	0.22	Boninsegna et al. (1989)[7]
Lago Róbalo	LRB	54°58'S/ 67°41'W	305	1489-2008	124	76	**0.80**	Llancabure (2011)[8]
Lagarostrobos franklinii								
Mt. Read	JMR	41°51'S/ 145°32'E	950	-2145-1999	344	176	**0.79**	Cook, et al. (2006)[9]
Lake Marilyn High	LMH	42°20'S/ 146°00'E	800	1542-1992	23	14	**0.88**	Buckley et al. (1997)[10]
Lake Marilyn Low	LML	42°12'S/ 146°00'E	700	1058-1992	24	12	**0.87**	Buckley et al. (1997)[10]
Phyllocladus aspleniifolious								
Blue Tier	BLT	41°12'S/ 147°58'E	750	1152-1994	84	43	**0.84**	Allen et al. (2001)[11]
Ralph's Falls	RFR	41°19'S/ 147°50'E	850	1240-1994	27	15	**0.79**	Allen et al. (2001)[11]
Race Course Spur	RCS	41°29'S/ 145°44'E	550	1467-1994	64	36	**0.91**	Allen et al. (2001)[11]
Kiaora	KAO	41°52'S/ 146°06'E	750	1598-1994	39	29	**0.78**	Allen et al. (2001)[11]
Mt. Arrowsmith	ARR	42°12'S/ 146°04'E	800	1541-1998	36	28	**0.83**	Allen et al. (2001)[11]
Scott's Peak Rd.	SPR	42°50'S/ 146°20'E	600	1519-1995	52	30	**0.82**	Allen et al .(2001)[11]
Site 600	SIX	43°00'S/ 146°33'E	600	1543-1998	35	23	**0.83**	Allen (2002)[12]
Halocarpus biformis								
Putara	PUT	40°42'S/ 175°31'E	650	1646-1993	38	21	0.37	D'Arrigo et al. (1998)[13]
Matiri Range	MAT	41°34'S/ 172°19'E	1060	1508-1999	51	28	0.51	Duncan et al. (2010)[14]
Mt. Glasgow	GLS	41°37'S/ 172°02'E	1050	1491-1999	48	26	**0.80**	Duncan et al. (2010)[14]
Croesus Track	CRS	42°17'S/ 171°23'E	900	1486-1999	52	35	**0.77**	Duncan et al. (2010)[14]
Mt. Elliot	MEL	42°30'S/ 171°50'E	1050	1440-1999	30	16	**0.90**	Duncan et al. (2010)[14]
Mt. Te Kinga	TKG	42°39'S/ 171°30'E	950	1450-1999	47	27	**0.88**	Duncan et al. (2010)[14]
Mt. French	MTF	42°40'S/ 171°20'E	750	1367-1999	56	31	**0.86**	Duncan et al. (2010)[14]
Camp Creek	CCP	42°43'S/ 171°34'E	970	1410-1998	72	53	**0.87**	Duncan et al. (2010)[14]
Mt Greenland	MGR	42°57'S/ 170°49'E	865	1400-1999	48	26	**0.87**	Duncan et al. (2010)[14]
Totora Saddle	TOS	42°59'S/ 170°51'E	210	1590-1998	32	20	0.42	Duncan et al. (2010)[14]
Mt. Bonar	BON	43°05'S/ 173°39'E	850	1463-1999	51	25	**0.83**	Duncan et al. (2010)[14]
Omoeroa Saddle	OMO	43°24'S/ 170°06'E	320	1578-1999	34	20	**0.63**	Duncan et al. (2010)[14]
Eldrig Peak	ELD	45°45'S/ 167°28'E	750	1338-1999	52	26	0.46	Duncan et al. (2010)[14]
Slopedown Hill	SPD	45°22'S/ 169°03'E	560	1447-1999	25	12	**0.70**	Duncan et al. (2010)[14]

UACH: Laboratorio de Dendrocronología, Facultad de Ciencias Forestales y Recursos Naturales, Universidad Austral de Chile, Valdivia, Chile.

CEQUA: Centro de Estudios del Cuaternario de Fuego Patagonia y Antártica, Punta Arenas, Chile.

SI_Table 2. Regional tree-ring chronologies.

Species	*Code*	*No. of series*	*No. of trees*	*Period*	*SD*	*Rbar*	*EPS ≥ 0.85*	*>30 series*
Austrocedrus chilensis	AUCH	853	554	1461-2003	0.188	0.183	1486	1558
Araucaria araucana	ARAR	758	386	1140-2006	0.314	0.245	1375	1409
Nothofagus betuloides	NOBE	275	181	1489-2008	0.196	0.119	1615	1633
Lagarostrobos franklinii	LAFR	344	176	-2145-1999	0.212	0.177	-1290	-1096
Phyllocladus aspleniifolius	PHAS	339	204	1152-1998	0.199	0.220	1435	1458
Halocarpus biformis	HABI	457	271	1367-1999	0.229	0.186	1445	1486

SD: Standard Deviation

Rbar: is the mean correlation coefficient for all possible pairings among tree-ring series from individual cores, computed for a specific common time interval. In this case we used a 50-year window with a 25-year overlap[15].

EPS ≥ 0.85: Early year with the Expressed Population Signal statistic ≥0.85, considered adequate to reflect a reliable common growth signal[16].

> 30 series: Early year with sample replication ≥ 30 series. We used this criterion to establish the chronology period suitable for developing the reconstructions (more severe than EPS ≥ 0.85).

SI_Table 3. Relationships between the regional chronologies and circulation indices from tropical (Southern Oscillation Index, SOI[17]) and extra-tropical (SAM) domains. Relationships significant at 95% confidence level are shown in bold red. *raw*: chronology without standardization, *std*: standard chronology, *res*: residual chronology[18].

Code	SOI (1948-1999)				SAM-Marshall[19]; *trendless* (n)	SAM-NCEP[20]; *trendless* (n)	SAM-Fogt[21] (n)	SAM-Jones[22] (n)
	DJF	MAM	JJA	SON	DJF	DJF	DJF	DFJ
AUCH-*raw*	0.09	0.09	-0.05	-0.05	**-0.57; *-0.45*** (47)	**-0.62; *-0.39*** (56)	**-0.33** (139)	**-0.38** (139)
AUCH-*std*	0.07	0.05	-0.07	-0.08	**-0.56; *-0.46*** (47)	**-0.58; *-0.39*** (56)	**-0.34** (139)	**-0.36** (139)
AUCH-*res*	0.06	-0.01	-0.14	-0.13	**-0.53; *-0.51*** (47)	**-0.46; *-0.47*** (56)	**-0.28** (139)	**-0.29** (139)
ARAR-*raw*	0.19	0.23	0.00	-0.09	**-0.55; *-0.41*** (50)	**-0.61; *-0.35*** (57)	**-0.32** (140)	**-0.38** (140)
ARAR-*std*	0.14	0.17	-0.05	-0.15	**-0.50; *-0.40*** (50)	**-0.55; *-0.37*** (57)	**-0.34** (140)	**-0.35** (140)
ARAR-*res*	0.19	0.25	0.02	-0.07	**-0.45; *-0.42*** (50)	**-0.37; *-0.33*** (57)	**-0.28** (140)	**-0.31** (140)
NOBE-*raw*	0.24	-0.04	-0.11	-0.26	**-0.51; *-0.39*** (51)	**-0.33**; *-0.19* (57)	**-0.19** (140)	**-0.27** (140)
NOBE-*std*	0.23	-0.07	-0.13	-0.26	**-0.50; *-0.38*** (51)	**-0.31**; *-0.20* (57)	**-0.19** (140)	**-0.24** (140)
NOBE-*res*	**0.42**	-0.02	-0.21	**-0.32**	**-0.37; *-0.37*** (51)	**-0.30; *-0.28*** (57)	**-0.18** (140)	**-0.19** (140)
LAFR-*raw*	-0.17	-0.19	-0.05	0.04	**0.34**; *0.15* (43)	**0.54**; *0.18* (52)	**0.20** (135)	**0.19** (135)
LAFR-*std*	-0.16	-0.14	-0.02	0.08	0.27; *0.11* (43)	**0.51**; *0.19* (52)	**0.18** (135)	**0.19** (135)
LAFR-*res*	-0.18	-0.16	-0.02	0.07	0.20; *0.15* (43)	**0.30**; *0.20* (52)	**0.18** (135)	**0.18** (135)
PHAS-*raw*	-0.21	**-0.32**	-0.14	-0.13	**0.34**; *0.08* (42)	**0.45**; *-0.03* (51)	0.14 (134)	**0.20** (134)
PHAS-*std*	-0.20	-0.24	-0.18	-0.15	0.20; *-0.02* (42)	**0.39**; *-0.04* (51)	0.08 (134)	0.15 (134)
PHAS-*res*	-0.10	-0.13	-0.14	-0.12	0.06; *0.05* (42)	-0.02; *-0.12* (51)	-0.01 (134)	0.06 (134)
HABI-*raw*	0.17	0.21	0.21	**0.28**	**0.49; *0.48*** (43)	**0.63; *0.48*** (52)	**0.38** (135)	**0.36** (135)
HABI-*std*	0.20	0.23	0.22	**0.29**	**0.46; *0.46*** (43)	**0.59; *0.47*** (52)	**0.38** (135)	**0.34** (135)
HABI-*res*	0.02	0.16	0.15	0.24	**0.33; *0.33*** (43)	**0.29; *0.34*** (52)	**0.38** (135)	**0.37** (135)

SI_Table 4. Southern Annular Mode (SAM) reconstructions. Calibration and verification statistics.

Calib. period	Predictand	Predictor	Calibration				Verification		Reconstr. length
			Adj r^2	F (s_e)	DW*d*	Residual Trend	RMSE*v*	*RE*	
1957-1999	SAM-Marshall[19]	PC1 of AUCH, ARAR, HABI	0.436	33.45 (1.087)	1.97	0.0266*	1.1014	0.41	1559-1999
1957-2003	SAM-Marshall	PC1 of ARAR, AUCH	0.373	28.40 (1.131)	2.08	0.0156^{ns}	1.1487	0.34	1559-2003
1957-1999	SAM-Marshall	PC1 of ARAR, HABI	0.350	23.63 (1.167)	1.70	0.0370*	1.1912	0.31	1486-1999
1957-2006	SAM-Marshall	ARAR	0.240	16.41 (1.230)	1.78	0.0160^{ns}	1.2604	0.19	1409-2006
1948-1999	SAM-NCEP[20]	PC1 of AUCH, ARAR, HABI	0.474	47.00 (0.699)	1.57	0.0202*	0.7093	0.45	1559-1999
1948-2003	SAM-NCEP	PC1 of ARAR, AUCH	0.388	35.87 (.749)	1.61	0.0184*	0.7596	0.36	1559-2003
1948-1999	SAM-NCEP	PC1 of ARAR, HABI	0.413	36.89 (0.739)	1.43	0.0230*	0.7534	0.38	1486-1999
1948-2006	SAM-NCEP	ARAR	0.291	23.75 (0.804)	1.47	0.0214*	0.8198	0.25	1409-2006

Adj $r^{2:}$ Coefficient of determination adjusted for loss of degrees of freedom.

F (s_e): F-value of regression; (S_e) standard error of the estimate

DW*d*: Durbin-Watson d statistic

RMSE*v* : the root-mean-square error of cross-validation.

RE: Reduction of Error

*: significant at 95% confidence level.

ns: not significant

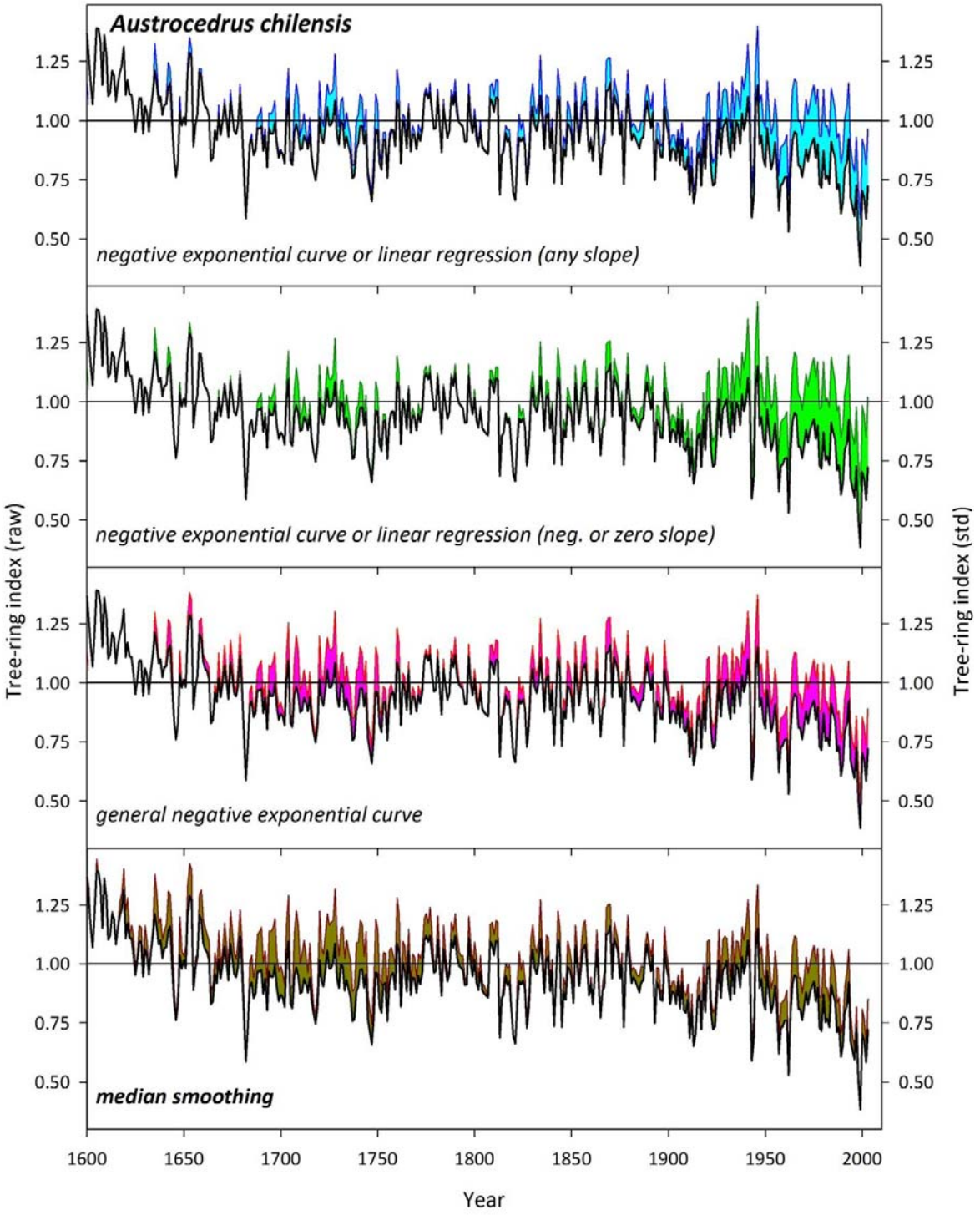

SI_Fig. 1. Comparison between the *Austrocedrus chilensis* raw tree-ring chronology without standardization (black line) and the chronologies produced using different curve fitting methods. The median smoothing method (**highlighted**) captures most of the variance in the low-signal frequency since 1950 contained in the raw chronology.

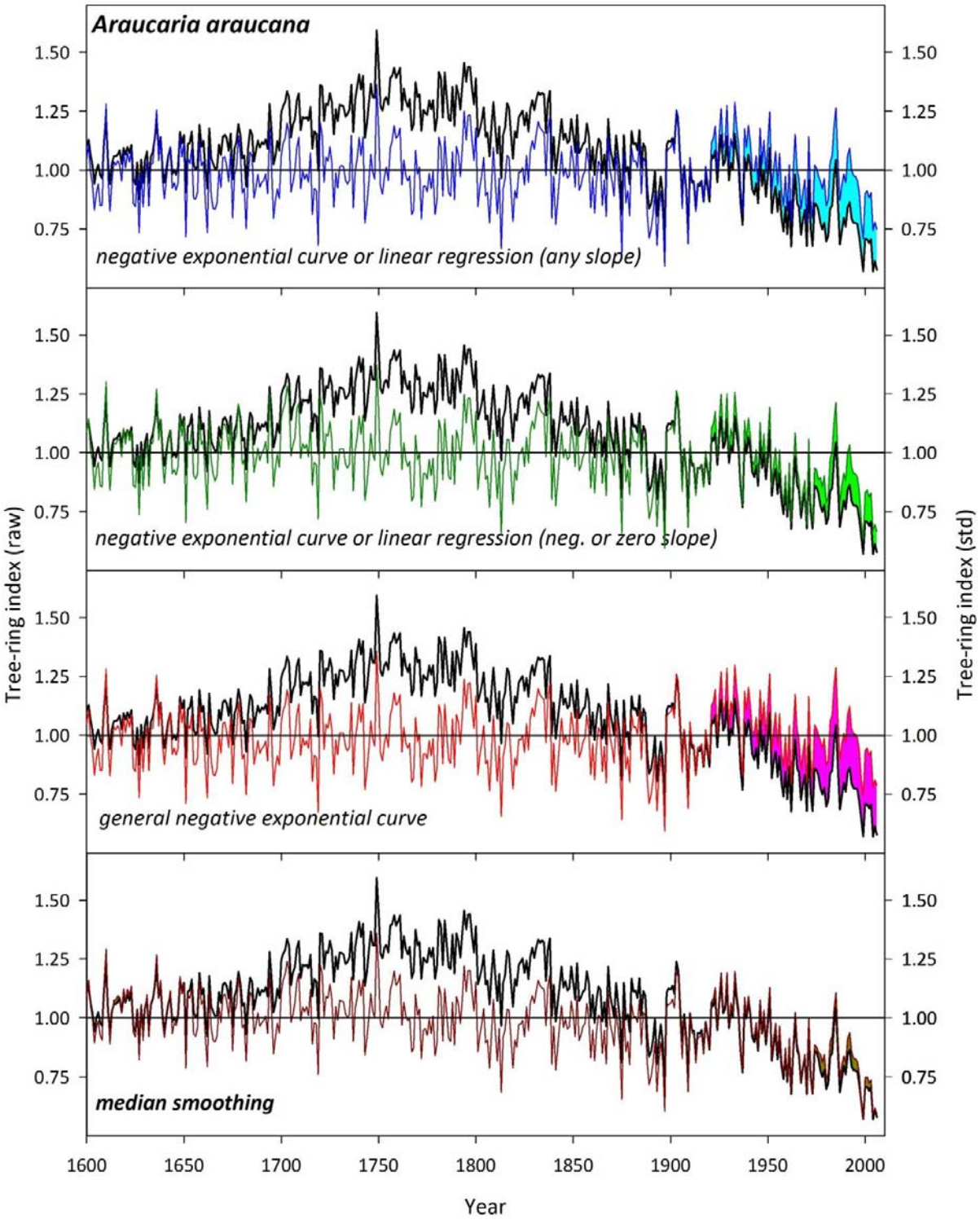

SI_Fig. 2. Same as in Fig. 1 for *Araucaria araucana*.

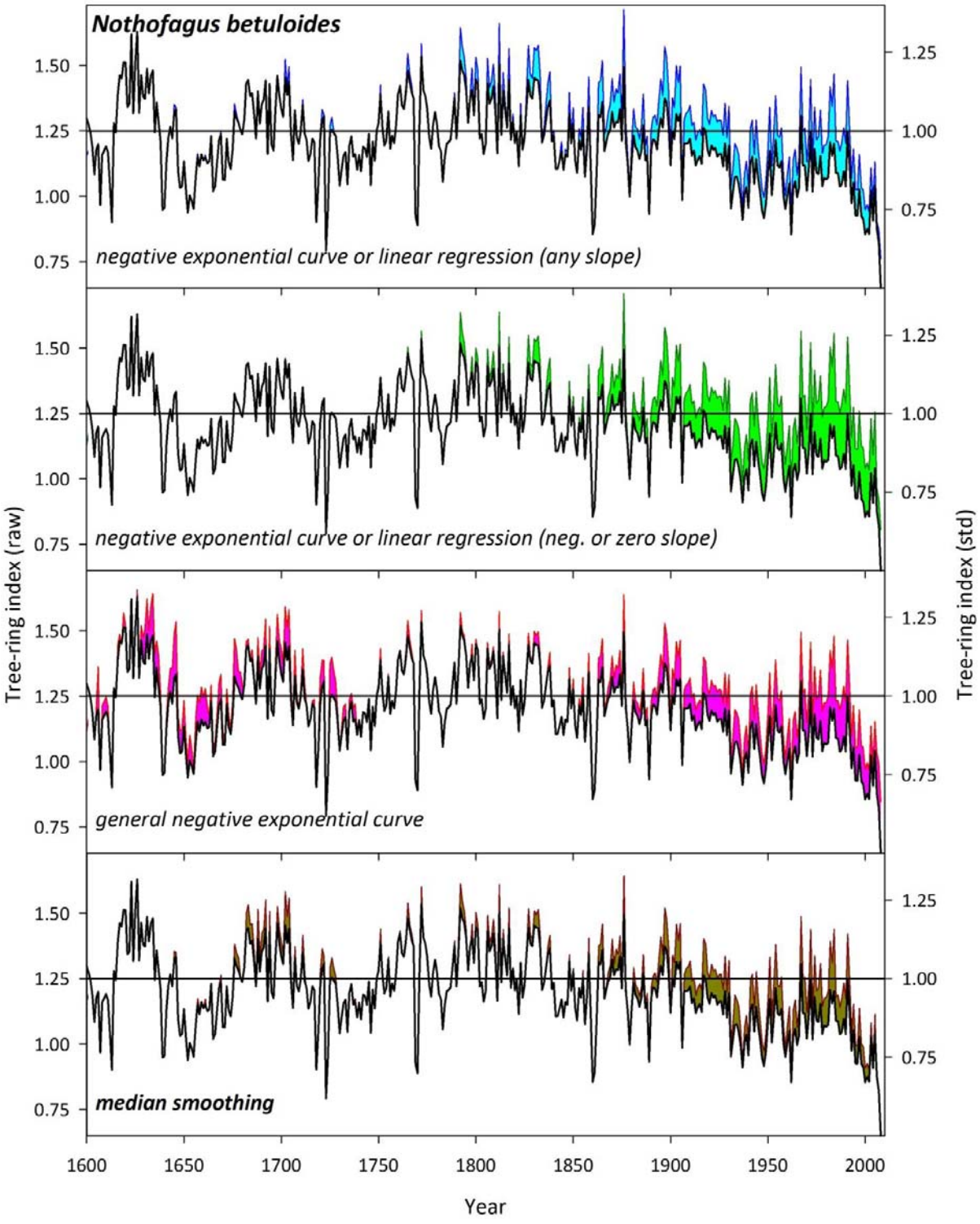

SI_Fig. 3. Same as in Fig. 1 for *Nothofagus betuloides*.

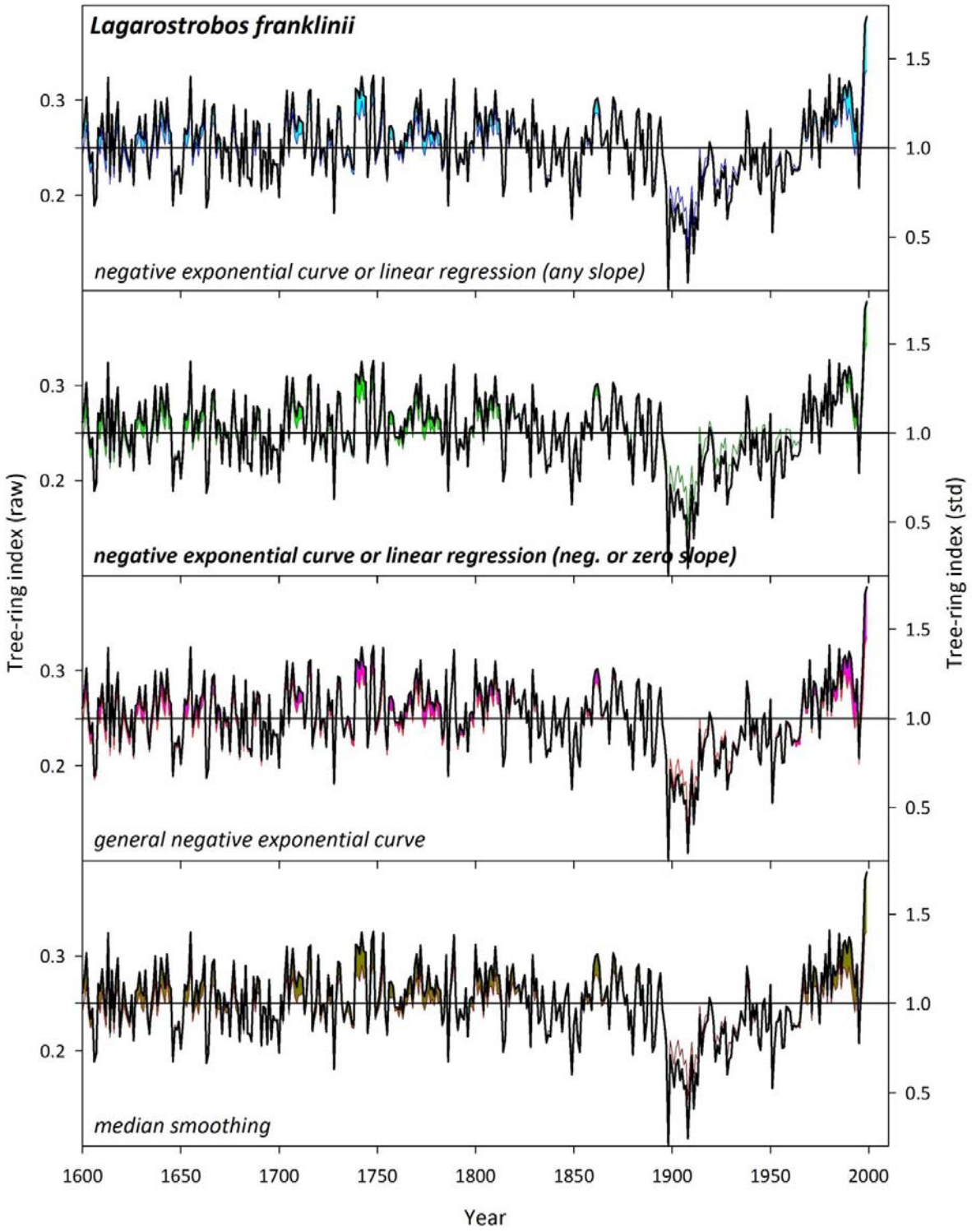

SI_Fig 4. Comparison between the *Lagarostrobos franklinii* raw tree-ring chronology without standardization (black line) and the chronologies produced using different curve fitting methods. The negative exponential curve or lineal regression with negative or zero slope (**highlighted**) captures most of the variance in the low-signal frequency since 1950 contained in the raw chronology.

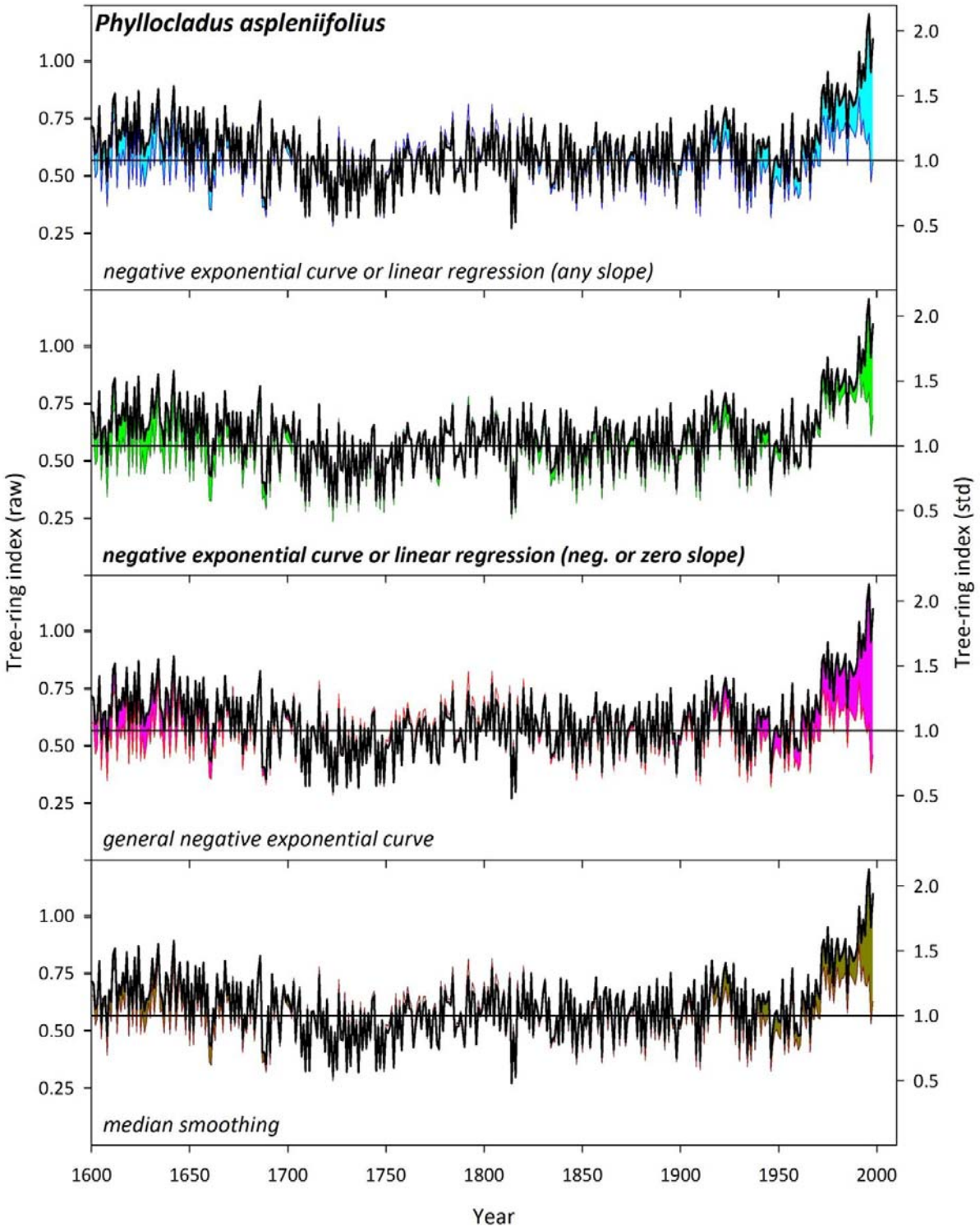

SI_Fig 5. Same as in Fig. 4 for *Phylocladus aspleniifolius*.

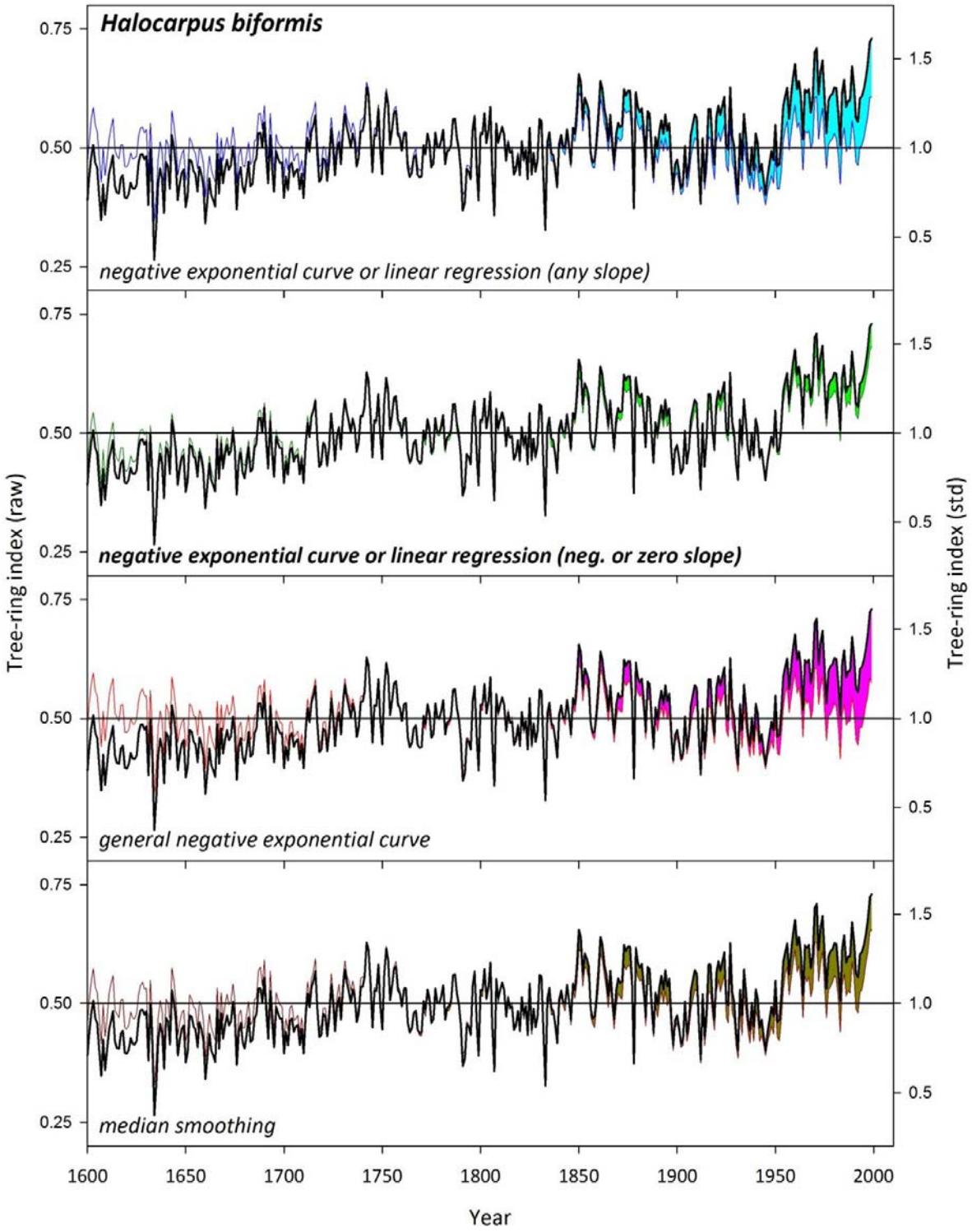

SI_Fig. 6. Same as in Fig. 4 for *Halocarpus biformis*.

Supplementary Information References

1. LaMarche, V.C., Holmes, R.L., Donwiddie, P. & Drew, L. Tree-ring chronologies of the Southern Hemisphere: 1. Argentina. Chronology Series V, vol 1. University of Arizona, Tucson. (1979).
2. Le Quesne, C., Acuña, C., Boninsegna, J.A., Rivera, A. & Barichivich, J. Long-term glacier variations in the Central Andes of Argentina and Chile, inferred from historical records and tree-ring reconstructed precipitation. *Paleogeogr. Paleoclim. Paleoecol.* **281**, 334-344 (2009).
3. Christie, D.A. Aridity changes in the Temperate-Mediterranean transition of the Andes since AD 1346 reconstructed from tree-rings. *Clim. Dyn.* **36**, 1505-1521 (2011).
4. Villalba, R. et al. Tree-ring based reconstructions of northern Patagonia precipitation since AD 1600. *The Holocene* **8**, 659-674 (1998).
5. Mundo, I.A., Roig Juñent, F.A., Villalba, R., Kitzberger, T. & Barrera, M.D. *Araucaria araucana* tree-ring chronologies in Argentina: spatial growth variations and climate influences. *Trees* DOI 10.1007/s00468-011-0605-3 (2011).
6. Villalba, R., Boninsegna, J.A. & Cobos, D.R. A tree-ring reconstructionof summer temperature between A.D. 1500 and 1974 in western Argentina. in: Third international conference on Southern Hemisphere Meteorology & Oceanography, Buenos Aires (1989).
7. Boninsegna, J.A., Keegan, J., Jacoby, G.C., D'Arrigo, R. & Holmes, R.L. Dendrochronological studies in Tierra del Fuego, Argentina. *Quat. South. Am.* **7**, 315–326 (1989).
8. Llancabure, J.J. Relaciones entre el crecimiento de *Nothofagus betuloides* y el clima local y de gran escala en bosques subantárticos de la Isla Navarino. Tesis Ingeniero Forestal, Facultad de Ciencias Forestales y Recursos Naturales, Universidad Austral de Chile (2011).
9. Cook, E.R. et al. Millennia-long tree-ring records from Tasmania and New Zealand: A basis for modelling climate variability and forcing, past, present and future. *J. Quaternary Sci.* **21**, 689-699 (2006).
10. Buckley, B.M., Cook, E.R., Peterson, M.J. & Barbetti, M. A changing temperature response with elevation for *Lagarostrobos franklinii* in Tasmania, Australia. *Clim. Change* 36**,** 477-498 (1997).
11. Allen, K.J., Cook, E.R., Francey, R.J. & Michael, K. The climatic response of *Phyllocladus aspelnifolius* (Labill.) Hook. f in Tasmania. *J. Biogeogr.* **28**, 305-316 (2001).
12. Allen, K.J. The temperature response in the ring width of *Phyllocladus aspelnifolius* (Celery-top pine) along an altitudinal gradient in the Warra LTER area, Tasmania. *Austr. Geograp. Studies* **40**, 287-299 (2002).

13. D'Arrigo, R.D. et al. Temperature-sensitive tree-ring records from New Zealand: long-term context for recent warming trend. *Clim. Dyn.* **14**, 191-199 (1998).
14. Duncan, R.P., Fenwick, P., Palmer, J.P., McGlone, M.S., & Turney, C. Non-uniform interhemispheric temperature trends over the past 550 years. *Clim. Dyn.* **35**, 1429-1438 (2010).
15. Briffa, K.R. in *Analysis of Climate Variability: Applications of Statistical Techniques.* (eds. Von Storch, H. & Navarra, A.) 77-94 (Springer, Berlin, 1995).
16. Wigley, T.M.L., Briffa, K.R. & Jones, P.D. On the average value of correlated time series with applications in dendroclimatology and hydrometerorology. *J. Clim. Appl. Meteorol.* **23**, 201-213 (1984).
17. Trenberth, K.E. Signal versus Noise in the Southern Oscillation. *Mon. Weather. Rev.* **112**:326-332 (1984).
18. Cook, E.R. A time series analysis approach to tree ring standardization. PhD. Dissertation, University of Arizonan Tucson, 185 pp. (1985).
19. Marshall, G. J. Trends in the southern annular mode from observations and reanalyses. *J. Climate* **16**, 4134–4143 (2003).
20. Thompson, D. W. J. & Wallace, J. M. Annular modes in the extratropical circulation. Part I: Month-to-month variability. *J. Climate* **13,** 1000-1016 (2000).
21. Fogt, R. L. et al. Historical SAM variability. Part II: Twentieth century variability and trends from reconstructions, observations, and the IPCC AR4 models. *J. Climate*, **22**, 5346-5365 (2009).
22. Jones, J. M. et al. Historical SAM variability. Part I: Century-length seasonal reconstructions. *J. Climate* **22**, 5319-5345 (2009).